A COMPARATIVE STUDY OF ELECTRON- AND POSITRON–POLYATOMIC MOLECULE SCATTERING

MINEO KIMURA

Graduate School of Science and Engineering, Yamaguchi University, Ube, Japan and Institute for Molecular Science, Okazaki, Japan

OSAMU SUEOKA

Graduate School of Science and Engineering, Yamaguchi University, Ube, Japan

AKIRA HAMADA

Department of Physics, Yamaguchi University, Yamaguchi, Japan

YUKIKAZU ITIKAWA

Institute of Space and Astronautical Science, Sagamihara, Japan

CONTENTS

Advances in Chemical Physics, Volume 111, Edited by I. Prigogine and Stuart A. Rice. ISBN 0-471-34990-9. © 2000 John Wiley & Sons, Inc.

I. INTRODUCTION

The aim of the present article is to draw a detailed comparison between the cross sections for positron- and electron–molecule collisions. The comparison is made on the basis of available experimental data for the positron- and electron–collision processes. Since many comprehensive reviews have been published on electron–molecule collisions, it will suffice to provide an introduction to positron–molecule collisions here.

The study of positron collisions with molecules has a long history. Interest in positron–molecule collisions arose from a study of positron

annihilation in a molecular gas and its related subject, the slowing down of a positron in a molecular gas. Due to rotational and vibrational excitation processes, molecules are more efficient than atoms for slowing down positrons, particularly at low incident energies. Using a simple model, Takayanagi and Inokuti [1] estimated rotational excitation cross sections for positron collisions with molecules. They demonstrated a significant difference between positron collisions and electron collisions in the process.

The simplest problem is the elastic scattering of a positron by a hydrogen molecule (H_2). Two groups of researchers addressed this problem in the early 1970s [2,3]. The first result of the measurement of the positron total scattering cross section for the molecules H_2, D_2, N_2, and CO was reported in 1974 [4]. The previous theoretical results turned out to be generally consistent with the experimental ones [5]. Throughout the late 1970s and the decade of the 1980s, theoretical and experimental studies of positron–molecule collisions were extensively made [6–13]. This work was reviewed by Kauppila and Stein in 1989 [14]. Emphasis in that review was placed on a comparison between positron and electron collisions, with the thought that such a comparison would help to provide a better understanding of the scattering of electrons by molecules. Electron scattering is of practical importance in many fields of application, such as astrophysics, plasma physics, gaseous electronics, atmospheric science, and radiation interaction with matter. On the theoretical side, Armour [6] summarized all the relevant works on positron–molecule collisions published up to 1988. He also drew a comparison between theory and experimental results [6].

Over the past decade, the scope of the theoretical and experimental treatments of positron collisions has become more and more elaborate. Cross sections have been measured for many large, complicated molecules (primarily by the group led by Sueoka, as described below in Section IV.A). Now differential cross sections (DCSs) are also available experimentally for molecules from the Detroit group led by Kauppila and Stein [15]. Experimental evidence of vibrational excitation of molecules has been obtained for CO_2 [16]. Sophisticated theoretical methods (e.g., the R-matrix method [17,18] and the Schwinger variational method [19,20]), which had been developed originally for electron–molecule collisions, have begun to be applied to positron collisions. It has long been established that positron scattering is highly sensitive to the effect of induced polarization. The accuracy of any theoretical result of positron–molecule collision hinges on the reliability of the model of polarization adopted for the calculation. Gianturco and his colleagues have developed a new approach to include the polarization effect [21], applying the method to calculations for various molecules e.g., H_2, N_2, CO, H_2O, and CO_2. Also, explicit account of

rotational and vibrational motions of the molecule is taken in the positron–molecule calculation under this approach [21].

Before proceeding to a detailed review of positron–molecule collisions, it may be useful to briefly summarize the characteristics of the problem, in comparison first to positron–atom collisions, and then to electron–molecule collisions.

The potential generated by a molecule is always anisotropic. Molecules have electric multipole (i.e., dipole, quadrupole, ...) moments. The interactions of an incident positron with these multipoles are usually anisotropic and of long range, a feature that constitutes one of the noticeable differences between the positron–atom and –molecule collisions. Molecules have rotational and vibrational degrees of freedom. If the interaction potential has a strong anisotropy, rotational motion can be easily excited. An anisotropic and long-range interaction between the incident positron and molecular multipoles is very effective in the excitation of molecular rotation. Molecular vibration is excited through the distortion of the electronic cloud of the molecule induced by the collision with the incident particle. In this sense, vibrational excitation is more sensitive to the short range part (i.e., near the molecular nuclei) of the interaction.

Dissociation of a molecule can be regarded as a limit of vibrational excitation. In many cases the dissociation products are reactive species (i.e., atoms and radicals). In this regard, the electron impact dissociation is of practical importance and has been studied extensively. Information is rarely available, however, on positron-impact dissociation. In relation to the dissociation process, the following process is of particular interest for a positron collision:

$$e^+ + AB \rightarrow A^+ + PsB, \tag{1.1}$$

This represents a dissociative positronium attachment, i.e., a positronium formation and attachment, followed by dissociation.

The production of PsH has been already reported [22]. This kind of Ps compound constitutes some interesting objects in atomic physics. Together they offer another test of many-body theory. A more challenging process is

$$e^+ + AB \rightarrow A \cdot e^+ + B, \tag{1.2}$$

representing a dissociative attachment of a positron to an atom. Very recently theory has shown that a Li atom can bind a positron [23]. Positron collisions with a Li-containing molecule could give experimental evidence of such an exotic positive ion.

The interaction potential between the positron or electron and a molecule consists of three components: electrostatic, exchange, and polarization. The static potential arises from the interaction between the projectile and the

electrostatic field of the molecule. Thus the static potential for the positron collision is the same as that for the electron collision except for its sign. There is no exchange interaction in the case of positron–molecule collision. Induced polarization plays a special role in the positron or electron collision with a molecule [24]. In the asymptotic (long-range) region, the polarization interaction for the positron–molecule collision is exactly the same as that for the electron–molecule collision. As the projectile comes closer to the molecule, the distortion of the molecular charge cloud becomes different for different projectiles. The polarization potential at short to intermediate range, particularly its anisotropic part, should be different for the two projectiles. As is mentioned above, the long-range interaction due to the molecular multipoles is important in the positron–molecule collision. The polarization interaction is another example of long-range interaction, but the cumulative effects of the two types of interactions are totally different for the two projectiles (additive for one and canceling for the other).

Due to the complexity of the potential, an electron may be temporarily captured by a molecule, giving rise to a so-called shape resonance in the electron scattering from considerable number of molecules. It is of interest to determine whether a similar resonance can occur in positron scattering. The shape resonance also affects the rotational and vibrational excitation processes. Even if no shape resonance occurs, the dependence on the projectile (i.e., positron vs. electron) can appear differently in the processes of rotational and vibrational excitation. A comparative study of positron– and electron–molecule collisions, particularly those increasing rotational and vibrational excitation (and dissociation), would be fruitful for understanding the dynamics of the interaction of both the positron and the electron with molecules.

In this respect, collisions involving polyatomic molecules are also of considerable interest. It is unlikely for a simple molecule to capture a positron and form a shape resonance. A large polyatomic molecule, however, may have some possibility of capturing a positron. A polyatomic molecule has multiple modes of vibration, and the dependence on the projectile may be different for different modes. For the same reason, preferable dissociation channels in the case of the positron–molecule collision may differ from those in the electron–molecule collision.

The present article is concerned more with polyatomic molecules than with diatomic and triatomic ones, which have been treated in general in an earlier review article [14]. A number of new and intriguing features recently observed for the first time for positron scattering from large polyatomic molecules are discussed herein and an analysis from combined theoretical and experimental points of view is provided.

All possible processes induced by electron and positron impacts are listed in Table I. For a view of the current status of the study of electron– and

TABLE I
Possible Processes for Electron and Positron Scattering

Initial[a]	Final	Processes
e_p+AB(v,J)	$\rightarrow e_p + \mathrm{AB}(v, J)$	elastic
	$\rightarrow e_p + e^- + \mathrm{AB}^+$	ionization
	$\rightarrow e_p + \mathrm{AB}^*(v,J)$	electronic excitation
	$\rightarrow e_p + \mathrm{AB}(v', J')$	rovibrational excitation
	$\rightarrow \mathrm{AB}^-$	electron attachment
	$\rightarrow \mathrm{AB}^{+-}$	positron attachment (not observed yet)
	$\rightarrow (e^+e^-) + \mathrm{AB}^-$	positronium formation (positron only)
	$\rightarrow h\nu + \mathrm{AB}^+$	direct annihilation (positron only)

[a] The term e_p represents either electron or positron.

positron–molecule collisions, the cross-section data currently available for all possible processes for electron– and positron–H_2 collisions are presented in Figures 1(a) and 1(b), respectively. For electron impact, a fairly large amount of data is available; those shown are the ones believed to be accurate or reasonable. Note that cross-section data for electron impact include total, momentum transfer, vibrational excitation to low-lying states, rotational excitation to low-lying states, electron attachment, electronic excitation, and ionization (with dissociative ionization), while those for positron impact are quite limited and are available only for total cross section, along with fragmentary data for positronium formation and ionization.

Section II provides a general review of the experimental method for positron collisions. Primary emphasis is placed on the method used by researchers at Yamaguchi University. The later discussion is mostly based on experimental results obtained by this group. An outline of the theory of electron/positron–molecule collision is given in Section III. The difference in interaction potentials between the two projectiles is elucidated. In Section IV, a detailed comparison of positron and electron collisions is presented for polyatomic molecules. A separate discussion of each of a number of different classes of the molecules is given. Section V presents some conclusions.

II. EXPERIMENTAL METHOD

A. Overview

Experimental methods of electron collisions have been reviewed many times; a very comprehensive recent monograph is also available [25]. Several review articles are available on positron collisions as well [10,14]. In this section, emphasis is on outlining the experimental method for positron scattering. In particular, details of the method used at Yamaguchi University

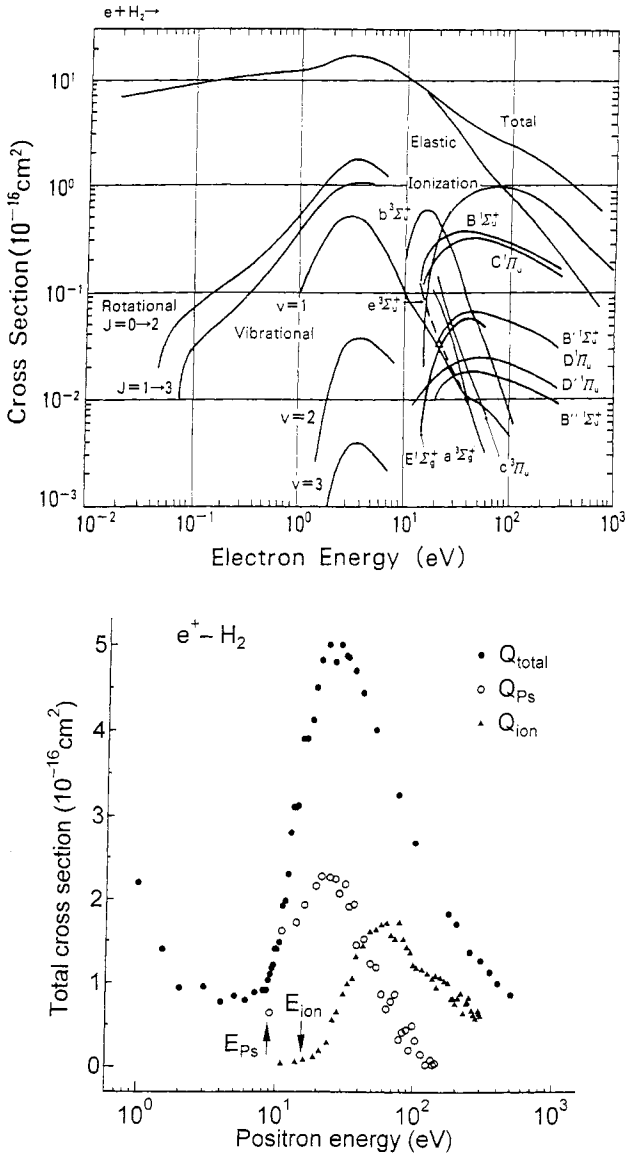

FIGURE 1. Available cross sections for various collision processes in H_2 molecule by electron impact (*a*), and positron impact (*b*). For electron impact, (*a*), cross sections for relatively large number of processes are established. From Ref. [26]. For positron impact, only those of total (Q_{total}), positronium formation (Q_{Ps}), and electronic excitation/ionization (Q_{ion}) at very limited energy region are available.

are described. The resulting cross sections are presented for discussion in Section IV.

The experimental method is described separately for total cross sections (Section II.B), cross sections for inelastic process (II.C), positronium formation (II.D), and elastic scattering (II.E). The total cross section (TCS) for a positron collision is defined by

$$Q_t^+ = Q_{\text{ela}}^+ + Q_{\text{ex}}^+ + Q_{\text{Ps}}^+ + Q_{\text{ion}}^+ + Q_{\text{dis}}^+ \tag{2.1}$$

where Q_{ex}^+ represents a sum of all the contributions from rotational, vibrational, and electronic excitations; Q_{Ps}^+ is the cross section of Ps formation, including contributions from ground as well as excited state formation; Q_{ion}^+ describes direct impact ionization; Q_{dis}^+ represents dissociation of a target molecule including the path through resonance or attachment; and Q_{ela}^+ is the elastic cross section. In general, a positron beam is spatially spread and energetically wide. It is difficult for the conventional technique developed for electron scattering to be used for the measurement of differential cross section (DCS) or any inelastic cross section. Only the measurement of Q_t has been made for a wide variety of atoms and molecules. In Section IV, the experimental result for Q_t for positron collisions is compared to the total cross section for electron collisions defined by

$$Q_t^- = Q_{\text{ela}}^- + Q_{\text{ex}}^- + Q_{\text{ion}}^- + Q_{\text{dis}}^- \tag{2.2}$$

The meaning of each component in the right-hand side is the same as in Eq. (2.1).

It is natural to believe that no special experimental technique is required for studying polyatomic molecules, as contrasted with atoms or simple diatomic molecules. A measurement for a polyatomic molecule can be made without much trouble as long as a sample is readily prepared in a collision cell. However, it is much more difficult to attain an understanding of the resulting experimental data in the case of polyatomic molecules, because a large number of channels are involved in the collision process. In Table II, the current status of the cross-section measurement for various processes carried out is presented, as well as corresponding cross-section data available for electron and positron impact.

B. Measurement of TCS for Positron Scattering

1. General Background

Many studies of TCS for positrons have been performed since the first development of a low-energy positron beam in 1972 [27]. Kauppila and Stein in Detroit used a high-energy proton beam impinging on boron targets to produce a ^{11}C positron source. In this case the boron target itself acts as a

TABLE II
Current Status of Experimental Studies for Electron and Positron Impacts

Type	Electron scattering[a]		Positron scattering[a]	
	Polyatomic Molecule	Simple Molecule	Polyatomic Molecule	Simple Molecule
Total (TCS)	△	○	△	△
DCS				
Elastic	△	○	△	△
Inelastic	△	○	—	—
Excitation				
Rotational	—	○	—	—
Vibrational	△	○	—	—
Electronic	—	○	—	△
Ionization	—	○	—	△
Positronium				
Formation			△	△
Scattering			△	△
Dissociation	—	○	—	—
Attachment	—	○	—	△

○: many studies; △: very limited study only; —: no study and hence, no data.

moderator. They made a systematic measurement of TCS for rare gas atoms [28,29]. They compared their positron cross sections with electron measurements. Their results have provided much insight into the scattering mechanism and have contributed to activity in this field. In the early period of the study, Au and MgO moderators were commonly used. Then, a tungsten (W)-moderator [30] was developed, leading to further progress of the positron beam experiment not only in positron–gas scattering, but also in positron–solid scattering. The W-moderator is convenient to handle and very effective. However, the rate of conversion of a fast beam to a slow one is as small as 3×10^{-4} even under a strong magnetic field and becomes less than 1×10^{-5} when producing a beam of better quality (i.e., a beam having a small perpendicular component to the flight path).

The TCS experimental study has been intensively carried out by several groups using their own techniques developed independently. Groups at University College London (UCL) [31], Wayne State University (Detroit) [14,28], and a few years later, those at University of Texas (Arlington) [32], Universität Bielefeld (Bielefeld) [33], and Yamaguchi University,[1] have started to carry out TCS measurements with useful accuracy.

[1] Positron and electron scattering experiments at Yamaguchi University by Sueoka were originally begun by Sueoka when he was on the faculty at the University of Tokyo, prior to his move to Yamaguchi in 1989.

2. *Experiment at Yamaguchi University*

Sueoka's group at Yamaguchi University has been vigorously engaged in TCS measurements for positron collisions, as well as electron collisions, with polyatomic molecules for a decade. Their experimental procedure and apparatus are described in the following [34,35].

a. Positron Source and Apparatus. A radioisotope ^{22}Na with activity of 50–100 μCi is used as a positron source. A W-ribbon moderator is placed as closely as possible to the source. The intensity of the slow positron beam can be maintained stable in a high-vacuum pressure (10^{-6} Torr) for a few months. A schematic diagram of the experimental set-up is illustrated in Figure 2. The experiment is based on the time-of-flight (TOF) method. The start signal is triggered by the photons emitted from the scintillation thin film upon impact by a fast positron from the source. The slow positron is detected by using a Ceratron, which is a kind of channel electron multiplier. The Ceratron detector can be used in a high pressure gas with up to 10^{-5} Torr. The length of the collision cell is set to be rather short, because the apparatus is intended to be used also for inelastic scattering experiments.

The gas pressure in the collision cell is controlled by a motor-driven method instead of a mass-flow meter, because the former is easier to use than the latter and can be used for any gas species. An electronic manometer

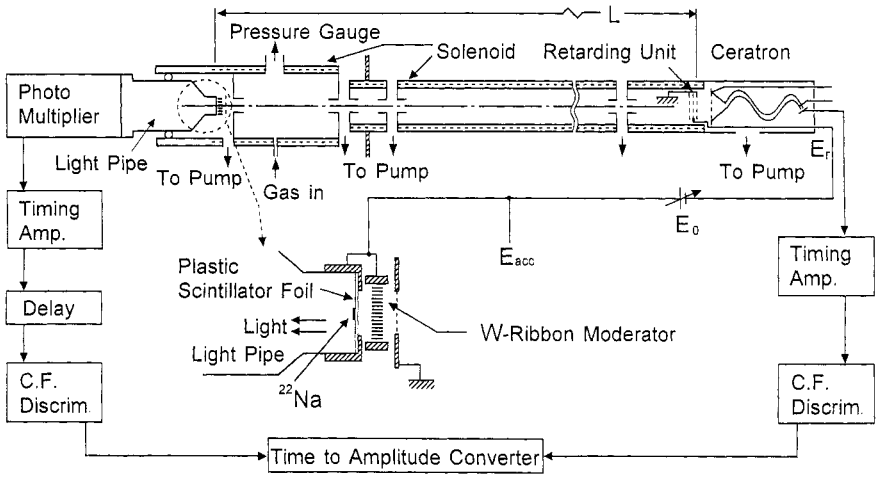

FIGURE 2. Schematic diagram of the experimental apparatus, and the main electronics. The abbreviated symbols are as follows; E_r, E_{acc}, E_0, and C.F. Discrim. are the retarding energy, acceleration energy, constant energy ($E_0 = E_{acc} - E_r$), constant fraction discriminator, respectively.

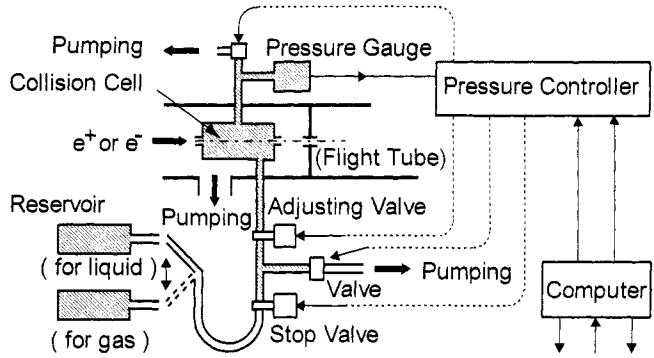

FIGURE 3. The gas supply system. The system was designed for fast evacuation at the changeover of the gas run to the vacuum run, and for the protection of the detector at the vacuum run to the gas run, respectively.

(Vacuum General: CMH4-M11) is installed as a pressure gauge. Any error of the pressure gauge is carefully monitored and considered in the normalization procedure of TCSs. The schematic diagram of the gas supply system is shown in Figure 3.

In an absorption-type measurement, it is important to avoid mixing of the scattered and unscattered beams. For this purpose, a retarding-potential grid is set in front of the detector to eliminate both the scattered projectiles with a large energy loss and those scattered elastically at large angles. One of the special features of the apparatus is an application of a magnetic field along the flight path for the transportation of the projectiles. It is not easy to select an appropriate strength of the magnetic field. If the field is too strong, then it causes too much forward scattering. On the other hand, if the field is too weak, then there is an extremely weak intensity of scattered positrons. The effect of the forward scattering is reasonably assessed by a simulation procedure, as described below. An example of the dependence of the TCS on the applied magnetic field is illustrated in Figure 4.

b. Energy Profile of the Projectile and the Calibration of the Energy. The energy spectra for the positrons and electrons used in these procedures are shown in Figure 5. They are obtained by the retarding-potential method. The spectra obtained from the TOF measurement are wider than those seen in the figure because of the low resolution of the TOF system.

For an electron beam, the resonance energies measured by the present TOF system for e^-–CO, e^-–CO_2 and e^-–N_2 collisions proved to be lower than the corresponding energies given in the literature. The difference in the resonance energies may be attributed to the component of the projectile energy that is perpendicular to the flight path. The averaged value of the

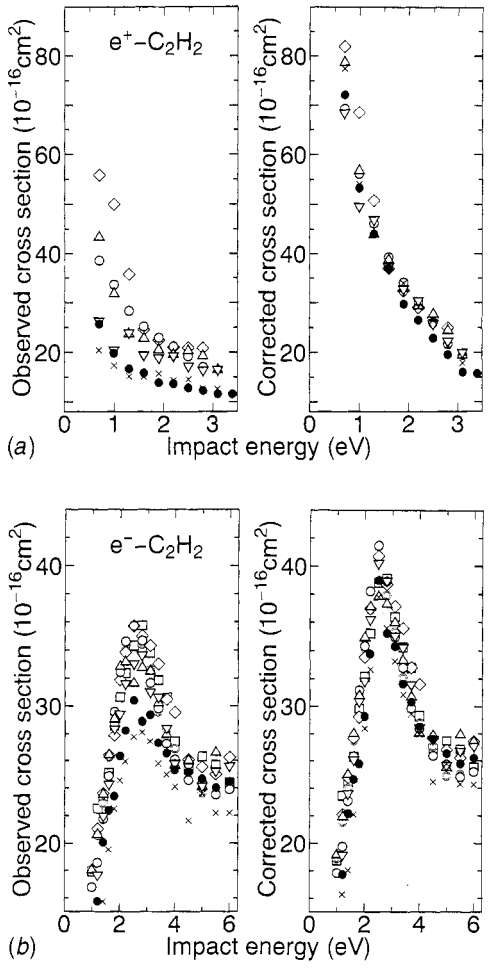

FIGURE 4. Observed cross sections and corrected cross sections for (*a*) positrons and (*b*) electrons colliding with C_2H_2. The corrected cross section data by the forward scattering effect in the method described in Section II.B.d which are shown in the right column should coincide with each datum-set in the magnetic field within errors after the correction. ◇, 3.6G; ○, 4.5G; △, 5.4 G; ▽, 6.8G; ●, 9.0G; ×, 11.3 G.

perpendicular energy was carefully examined and was found to be nearly independent of the beam energy. It is approximately 0.2 eV in the standard TCS measurement. In the case of the positron beam, the correction for the magnetic field effect is not considered, because no energy standard is known. However, the perpendicular component of the positron energy was found to be much smaller than that in the case of the electron beam.

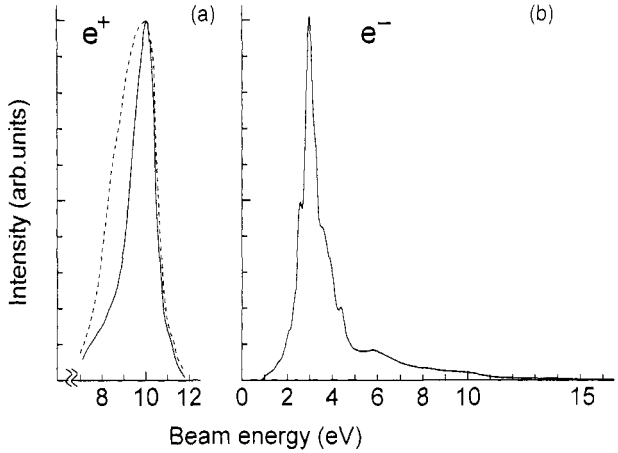

FIGURE 5. Beam profiles: (*a*) positron, and (*b*) electron. The positron spectrum was obtained by acceleration energy of 8.5 eV. In (*a*), measurement was taken soon after the moderator baking (*solid curve*) and a week after the baking (*dotted curve*). The moderator surfaces are perhaps covered with oil vapor. Small structures seen in the acceleration of 3.0 eV are probably due to the measurement error.

c. Data Analysis. True time spectra are deduced from the TOF data using an improved formula employed by Mori and Sueoka [36], which was originally derived by Coleman et al. [37]. The TCS is given by the relation

$$Q_t = -[1/(nl)]\ln(I_g/I_v), \tag{2.3}$$

where n and l are the gas density and the effective length of the collision cell, and I_v and I_g are the intensities of the projectile transmitted through the vacuum and the gas, respectively. The effective length is determined by normalizing the present TCS data for e^+–N_2 at the intermediate energies (15–200 eV) to those of Hoffman et al. [38]. The TCS measured is confirmed to be independent of the gas pressure. Examples of the pressure dependence of the cross section are shown in Figure 6.

In this sense, the measurement of Q_t by Sueoka's group is based on a "relative" technique. In the procedure, the effective length l is determined on the assumption that the pressure gauge gives an accurate absolute value. Therefore, special care must be taken in the pressure determination. The value of l thus determined is found to almost coincide with the geometrical length of the cell. It can be safely concluded that the pressure gauge used is very stable, because almost the same effective length has been obtained for many measurements with the same geometrical condition of the collision

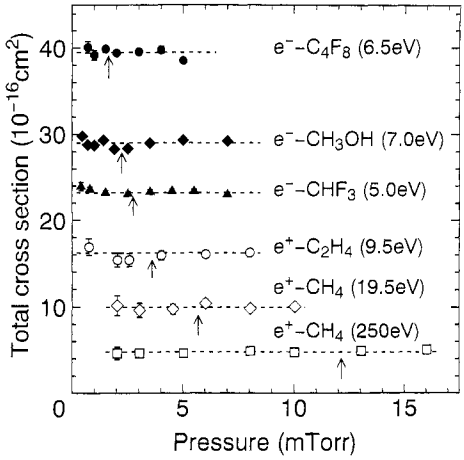

FIGURE 6. Total cross sections plotted against gas pressure. Error bars shown only include the statistical error. The numbers in parentheses correspond to the impact energy. All present TCS measurements were normally carried out at the pressure indicated by the arrow.

cell carried out by this group over a period of a decade. This also confirms the reliability of the experimental data obtained by the Detroit group.

d. Forward Scattering Correction. Because a wide exit aperture is employed in the present TOF system with a magnetic field for the beam transportation, the effect of forward scattering is not expected to be small. If we take into account the effect of forward scattering, the intensity I_g in Eq. (2.3) should be changed to $[I_g - I_f]$, where I_f is the intensity corresponding to the forward scattering [39]. Generally it is not easy to obtain the quantity I_f. The calculation of I_f is based on whether the particle scattered inside the collision cell passes through the exit aperture. Then we have

$$I_f = [1/(\pi y^2 Q_t)] \int dI(x) \int 2\pi r\, dr \int \Phi(\theta, r, x, E, B) q(\theta) \sin\theta\, d\theta \qquad (2.4)$$

where y represents the radius of the aperture, and Φ is the transmittance function of the cell and depends on the beam energy, E, the magnetic field, B, the distance from the scattering point, x, the radial distance from the center of the scattering cell, r, and differential cross section, $q(\theta)$. In the above equation,

$$dI(x) = I_0\{\exp(-Q_t n x) - \exp[-Q_t n(x + dx)]\} \qquad (2.5)$$

Thus the Q_t is self-consistently determined by solving Eq. (2.3) by replacing I_g by $[I_g - I_f]$, and solving Eq. (2.4) by using Eq. (2.5).

For strongly polar molecules such as H_2O and HCl, the Q_t values are significantly affected by the forward scattering. Good agreement of the corrected data with the theoretical result can only be attained when the theoretical calculation is carried out taking explicit account of the effect of the dipole interaction [40]. Good agreement with the theory [41] for H_2O suggests that the present procedure for simulating the forward scattering correction is reasonable and plausible.

C. Inelastic Scattering of Positron

1. Overview

Recently, impressive progress has been achieved in making measurements for inelastic processes, such as electronic excitation, Ps formation, and ionization, though researchers are still far from having a complete understanding of the mechanisms. The experimental studies show energy dependence of cross sections (e.g., threshold behavior) for each process. Together with the comparative studies of electron, proton, and antiproton impact, they provide much insight into collision dynamics. However, very few experimental studies have been reported for polyatomic molecules. This paucity is the result of many inelastic channels being involved in the collision system.

In this subsection, we review the experiments done on inelastic scattering. The discussion is divided into two parts from the technical point of view, depending on the intensity of the positron beam being treated. The boundary between a weak and a strong source is roughly 100 μCi of the source.

2. Experiment Using a Weak Positron Source

The first inelastic scattering experiment with a positron beam was performed with a TOF system by Griffith et al. [42]. Their method was originally developed for a study of electronic excitation of He by Coleman and Hutton [43]. Sueoka [44] carried out a similar experiment to measure ionization and electronic excitation cross sections for He. It is based on the measurement of the TOF spectra of the inelastically scattered positron. The advantage of the method is good efficiency of the measurement, while its main disadvantage is an incomplete collection of the scattered positrons, even with the application of a strong magnetic field. In the case where the forward scattering dominates, this method works well and provides reasonably good results. Ionization and excitation of rare gases obey such a condition, and so a weak source is suitable for the study. The method was applied to the study of the Schumann–Runge excitation of O_2 [45]. Since this

excitation occurs in a broad band, the measurement using a positron beam with an energy width of 2 eV is feasible and was indeed successfully made. Sueoka and Mori [46] have also tried an inelastic scattering measurement of positron impact on H_2O and NH_3 molecules. However, the TOF spectra for these molecules were found to be rather broad and ambiguous, and consequently the resolution of the positron spectra was much poorer than that of electron spectra. No definite result was obtained for these systems.

As a matter of practice, whenever an attempt is made to measure a TCS for a polyatomic molecule, Sueoka's group tries an inelastic scattering measurement for the molecule, as a supplemental measurement. Figure 7 shows an example of inelastic spectra for SiH_4 upon positron impact [13], compared with the corresponding electron energy-loss spectra [47]. In this case, the spectrum shows no structure below the energy of 8.0 eV, while the structures due to the energy loss above 8.0 eV are not well separated. Such a crude spectrum can readily be obtained, but it is difficult to extract meaningful information from it. As described below, a measurement of ionization or Ps formation cross section can be performed with better accuracy using a stronger positron source. For electronic excitation, however, no method other than the experiment with a weaker source has been developed so far.

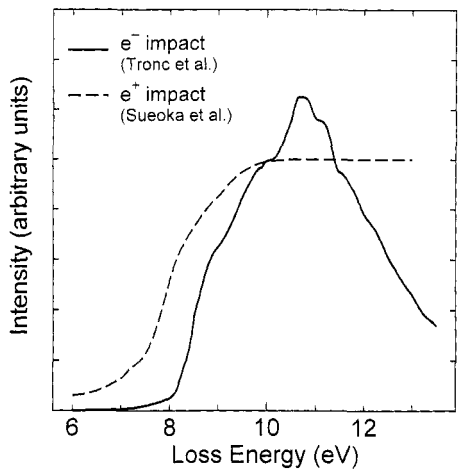

FIGURE 7. Energy loss spectra of positron and electron impacts from the valence-shell of SiH_4 [47]. The electron spectrum was recorded with 25 eV incident at $\theta = 0^\circ$ scattering angle. The positron spectrum was obtained from the TOF measurement used for TCS experiments under the stronger magnetic field.

3. *Experiment Using a Strong Positron Source*

Because of extremely weak intensity or low brightness of the positron beam, a standard experimental method developed for inelastic scattering of electron beam is not easily applicable to positron scattering, even with a strong positron source. A strong source has the advantage that a coincidence measurement is possible, but for electronic excitation, the coincidence method is unusable. The Bielefeld group developed a skillful experimental method based on a coincidence technique to measure total ion yield and a positron–ion correlation with a strong positron source [48]. In the measurement, both the ionization Q_{ion} and the Ps-formation Q_{Ps} cross sections are obtained simultaneously.

Moxom et al. [49] at UCL measured total ionization cross section for He, Ar, and H_2 with a strong positron source. By improving the method, they succeeded in making a precise measurement of the single ionization cross section in the vicinity of the threshold [50]. The threshold behavior of the cross section in the electron scattering has been studied extensively, and is known to obey the Wannier threshold law. The threshold law for ionization is now established as,

$$\sigma_{\text{ion}} \sim (E - E_{\text{ion}})^n \tag{2.6}$$

For electron scattering, the exponent is known to be $n = 1.127$. Ashley and co-workers [50] determined the exponent for positron scattering for the first time. Their values, $n = 1.99 \pm 0.19$ and 1.70 ± 0.11 for He and H_2, respectively, are found to be larger than those for electron by Wannier theory, but smaller than the theoretical value of Klar [51]. More recently, Ihra et al. [52] investigated threshold behavior of ionization for positron scattering from He and H_2 and provided a rationale.

D. Positronium (Ps) Formation

1. *Overview of the Ps Formation Experiment*

Ps formation cross sections, Q_{Ps}, were first obtained for He, Ar, H_2, and CH_4 by Charlton et al. at UCL using a measurement of the 3 γ-ray photons in coincidence resulting from the self-annihilation of *ortho*-Ps [53]. Since then, a variety of experimental data on Q_{Ps} have been reported by various groups. Fornari and co-workers of the Arlington group measured absolute cross sections for Ps formation for He, Ar, and H_2 by observing the scattered positrons [54,55]. In their experiment, the number of Ps formations was obtained by counting the reduction of the scattered positrons (backward scattered positrons being measured by repelling them from the backward region) from the incident ones. Their data were found to be larger by a factor

of three than those obtained by the UCL group, and they also showed a different energy dependence. The data of Arlington group does not have the sharp peaks seen in the UCL measurements. However, recently the UCL group found the systematic errors in their early measurements [10].

As is described in Section II.C.3, the Bielefeld group measured Q_{Ps} for positron scattering from He and H_2 by measuring both the total ion yield and the number of positron–ion coincidences [48,56]. The resulting Q_{Ps} for H_2 in particular shows a reasonable accord with the data of the Arlington group [57]. They are also in accord with the theoretical ones by Bussard et al. [58]. Very recently, the Detroit group has successfully carried out the measurement of Ps-formation cross section for rare gases and some molecules including CO_2, CH_4, and SF_6 [59]. Their method is based on the coincidence technique to detect the two 511-keV annihilation gamma rays, and the transmission of the positron beam through the gas scattering cell [60]. The results for rare gases are compared with those by the Arlington group. The agreement has been found to be generally good as far as the comparison can be made. Furthermore, they have observed structures in the energy dependence of Q_{Ps}. Although the exact cause of the structure is not known, it may well be due to contributions from the electrons in different atomic and molecular valence shells, which possess different Ps-formation thresholds within a narrow band of a few eV.

2. *Ps Formation Measurement Based on the Hybrid Method at Yamaguchi University*

Measurements of Q_{Ps} for molecules have been made so far only for CO_2, CH_4, and SF_6 molecules [59] [61]. Certainly, a more systematic and comprehensive study is needed to understand the characteristics of Ps formation in polyatomic molecules.

In the energy dependence of the TCS in the case of rare gases, a sudden increase of the cross section is clearly seen just above the Ps formation threshold [29]. For some of the polyatomic molecules studied at Yamaguchi University, however, this distinct feature does not necessarily appear, or the feature is significantly weakened or washed out. To understand this finding, an alternative type of experiment was performed on the basis of the combination of the TCS experiment of conventional absorption type [34], and the Ps formation experiment similar to that of the Arlington group [11]. Specifically, the absorption-type TCS experiment was performed with a stronger magnetic field. The contribution of Ps formation was found to be enhanced in the cross-section curve, because the forward scattering was increased further. As an example, representative cross sections for C_2H_2, C_2H_6, C_3H_8, and C_3F_8 are shown in Figure 8.

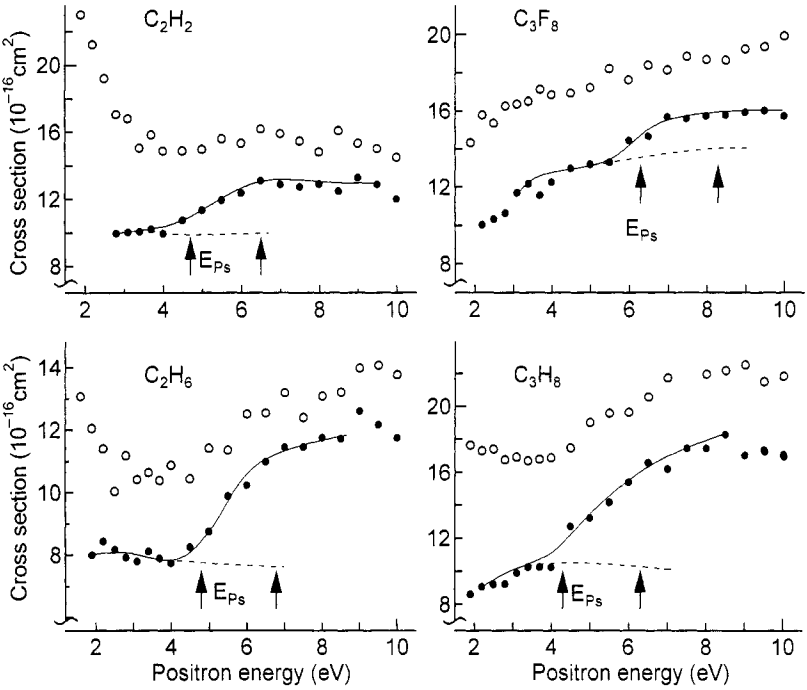

FIGURE 8. Illustration of the estimation of Ps formation cross section in C_2H_2, C_2H_6, C_3F_8, and C_3H_8. Open circles are the TCS data uncorrected by the forward scattering effect. Closed circles are the observed cross-section data under a strong (31 Gauss) magnetic field. Extrapolation of the contribution of observed cross section is shown (*dashed curve*). The area between the curve and the TCS is the cross section of Ps formation. Arrows show the threshold energy of Ps formation, E_{Ps} and the position of 2 eV above from the E_{Ps}.

The ratios of Q_{Ps} to the total cross section at 2 eV above threshold are tabulated in Table III for a number of molecules. The data contain interesting information regarding the contribution of Ps formation to TCS, and may lead to possible new physics. This subject is discussed in Section IV.

E. Elastic Scattering

1. Overview

Elastic scattering is the only collision process below the rovibrational excitation threshold, where the elastic cross section is equal to the total cross section. Recently, interest has arisen in the threshold behavior of the elastic cross section. In the cases of rare gases and simple molecules, a cusp in the elastic cross section at the Ps formation threshold (E_{Ps}) has received considerable attention theoretically and experimentally [62,63]. There still remains a controversy about the existence of the cusp. In the cases of

TABLE III
The Ratio of the Cross Section of Ps Formation (Q_{Ps}) to TCS (Q_T) in Per Cent (%) at 2 eV Above Each Threshold[a]

Molecules	Q_{Ps}/Q_T (%)
CH_4	25
C_2H_2	13
C_2H_4	17
C_2H_6	23
C_3H_8	21
CH_2F_2	4.0
CHF_3	5.9
C_2F_6	4.8
C_3F_8	4.4
C_4F_8	8.2
CO_2	8.1
OCS	9.3
SF_6	8.6
H_2O	2.3
NH_3	2.9
HCl	5.8
HCOOH	6.5
CH_3COOH	6.5
C_6H_6	5.1
$C_6H_5CH_3$	7.9
CCl_4	14
CH_3OH	8.5
C_2H_5OH	6.2

[a] New data for this review. O. Sueoka, and M. Kimura [64].

polyatomic molecules, a precise measurement of TCS in the vicinity of E_{Ps} is still a difficult task.

2. *Differential Cross Sections of Elastic Scattering*

Since a positron beam is essentially of low brightness, a DCS measurement requires the immense effort of a long time spent on measurement. The Detroit group was the first to measure the elastic DCS for rare gases successfully using a crossed beam geometry [12,65]. Using the same experimental apparatus, DCSs for electron scattering were measured in order to test the experimental system. Their experimental setup is shown in Figure 9. As a positron source, a radioisotope ^{22}Na with an activity of 150 mCi was employed. A positron beam of variable energy with an energy width of about 2 eV was obtained from an annealed tungsten moderator placed in front of the positron source. The electron beam with an energy width of several eV was produced as a secondary electron from the same

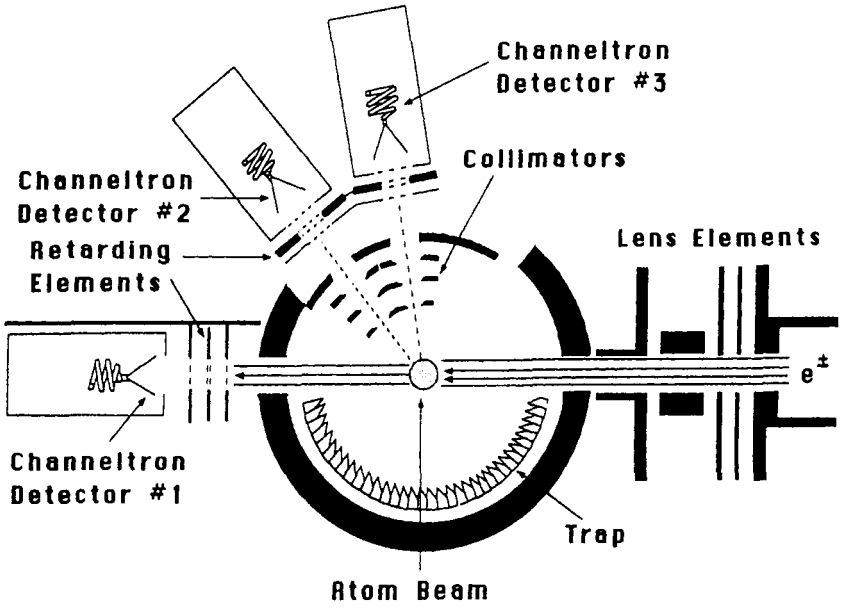

FIGURE 9. Experimental setup for DCS of the Detroit group. From Ref. [12].

moderator. The projectile beam is crossed with a molecular beam effusing from a multichannel capillary array. The primary beam is monitored using the channeltron detector #1. The scattered projectiles are detected by using two rotary channeltron detectors #2 and #3 at angles from 30° to 135° with an angular acceptance of $\pm 8°$. The retarding element placed in front of the detector is used to determine the energy distribution of the primary beam and to exclude the scattered projectiles that lose their energy by more than 1 eV.

For a polyatomic molecule, quasi-elastic (elastic plus rotational and vibrational excitations) DCSs for e^+– and e^- – CH_4 collisions at 4 to 200 eV were reported recently by the Detroit group [66]. The DCS measured for e^-–CH_4 were normalized at 90° to the experimental data of Boesten and Tanaka [67] (elastic plus rotational excitations) at 15 and 20 eV, and to the measurement of Sakae et al. [68] (elastic plus rotational and vibrational excitations) at 200 eV. The normalized data are found to be in good accord with other recent results for electron scattering.

The experimental data on the quasi-elastic DCS for e^+–CH_4 collision are shown in Figure 10 together with the electron scattering data of Boesten and Tanaka [67]. The data at 6, 10, 50 and 200 eV were normalized at 90° to those of the theoretical calculation of Jain and Gianturco [69]. The general shape of the normalized DCSs agrees qualitatively with the theoretical

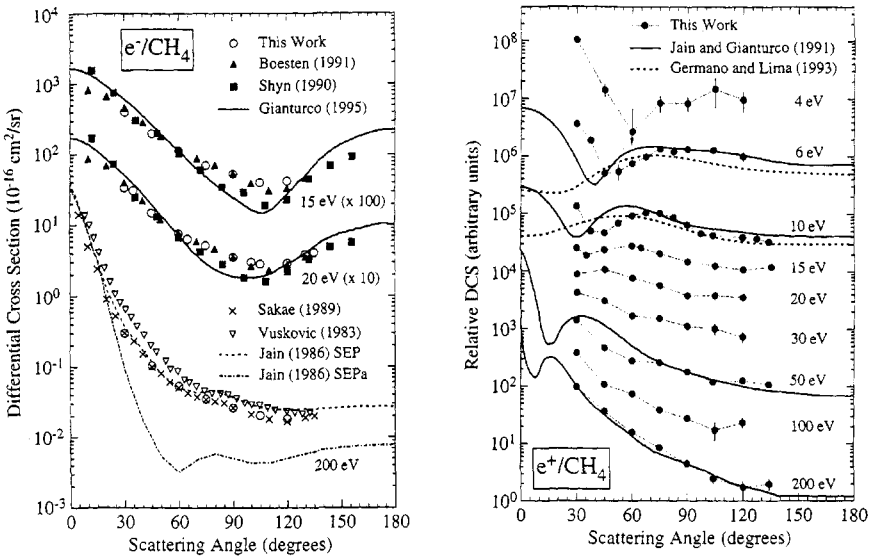

FIGURE 10. Differential cross sections for e^-–CH_4 at 15, 20, and 200 eV, and e^+–CH_4 at 4, 6, 10, 15, 20, 30, 50, 100, and 200 eV obtained by the Detroit group [66].

behavior, while the minima appear at smaller angles in the theoretical cross sections than those in the measured result. The minimum in the DCS near 60° at 4 eV shifts towards smaller angles and becomes shallower with increasing energy. The behavior of the measured DCS is very similar to the elastic DCS for e^+–Ar [65]. The Bielefeld group [9] measured an elastic DCS for positron impact on Ar gas by using a crossed-beam apparatus. This is a more standard approach for a DCS measurement than that of using the apparatus of the Detroit group and may offer correspondingly better accuracy than the latter. To date, however, no report on molecular targets has appeared from the Bielefeld group.

3. *DCS Measurement Using an Axial Magnetic Field*

In a transmission-type experiment, it is possible to extract information of angle dependence from the resultant data by using an axial magnetic field. Coleman and co-workers reported the DCS data for e^+–Ar scattering obtained from a TOF spectrum under a strong magnetic field of 140G [70]. For e^+–and e^-–H_2O scattering, the DCS at small angles was estimated from the dependence of the cross section on the magnetic field strength by the Yamaguchi group [39,40]. The experimental data agree with the theoretical electron-scattering data, which were obtained by applying the first Born approximation.

F. Positron Experiment in the Future

As described above, the measurement technique of TCSs for positron impact has emerged from its infancy and been applied to a variety of systems successfully. However, inelastic scattering and differential cross-section experiments do encounter a difficulty, one inherent in the low brightness of the positron beam. For the positron scattering experiment, a high quality beam of high brightness is desirable, especially for polyatomic molecules because of their complicated energy spectra. A method of brightness enhancement (BE) of positron beam has been developed for a study of a solid surface [71]. The BE method is based on the double reflection type and needs an ultrahigh vacuum. On this point, the scattering experiment for a gas target becomes less advantageous, but it may still be possible if employing the differential pumping technique. The high quality beam by the BE method may be attainable for the energy width of less than 0.1 eV and the beam diameter of less than 0.3 mm. The high quality beam is also useful for the TCS measurement at extremely low energies. Use of the BE method in conjunction with a stronger radioisotope would greatly enhance the progress in positron scattering experiments and could be expected to help begin a new era of experimental research for positron scattering.

III. THEORETICAL ASPECTS OF ELECTRON AND POSITRON SCATTERING

In this section, the framework of theoretical models and approximations used for calculating cross sections for electron or positron impacts on molecular targets is summarized. In particular, the *difference* and *similarity* between approaches for electron and positron scattering are highlighted, thus providing a basis for the discussions of experimental results that follow in later sections. As will be seen, the most essential, and crucial, part of the theory for determining dynamics correctly is the area of interaction potentials, and therefore a good deal is devoted to discussion to them. First, the two opening sections briefly summarize the outline of the theoretical framework, which are then followed by discussion of the interactions. Readers who are interested in more details of theories are encouraged to read the review article by Lane [72].

A. Hamiltonian and Scattering Dynamics

1. Hamiltonian

The time-independent theory of electron or positron scattering is based on a stationary state description of continuum states of the electron/positron-plus-

target system. The objective is to calculate wave functions of the electron/positron–molecule Hamiltonian,

$$H = T + V_{\text{em}} + h_{\text{M}} \tag{3.1}$$

where T, V_{em}, and h_{M} represent the kinetic energy of the projectile, the electron– or positron–molecule interaction potential energy, and the Hamiltonian of the isolated target molecule, respectively. Provided all the interactions are reasonably well known, the next question is how to solve this Schrödinger equation with a reasonable approximation, but without losing too much of the principal elements of the underlying physics.

2. *Scattering Dynamics*

From a classical point of view, a fast collision is one in which the collision time is much shorter t_{c} ($<10^{-15}$ s) than the periods for nuclear rotation t_{R} ($>10^{-12}$ s) or vibration t_{v} ($>10^{-14}$ s), so that the nuclear motion thus has little movement during the collision, and it is a reasonable approximation to treat the nuclei as held fixed (the Franck–Condon principle). Then it is only necessary to consider the electronic Hamiltonian for the electron– or positron–molecule system for studying dynamics. Thus, the total wave function may be represented by a product of electronic and nuclear wave function. Several approaches have been employed to solve the scattering equation; some of those most commonly used are briefly summarized below.

a. Direct Close-Coupling Method. It is usually common practice to obtain the total wave function by an expansion in terms of the complete set of unperturbed states of the isolated molecule, viz.

$$\Phi(\mathbf{r}, x) = \mathscr{A} \sum F_{\text{i}}(\mathbf{r}) X_{\text{i}}(x), \tag{3.2}$$

where $\mathscr{A}$ is the usual antisymmetrization operator for electrons, and of course, no antisymmetrization procedure is necessary for positrons. In principle, the summation in Eq. (3.2) includes all continua as well as bound states of the target. The one-electron scattering functions F satisfy the set of coupled equations

$$[\Delta + k_{\text{n}}] F_{\text{n}}(\mathbf{r}) = 2 \sum [V_{\text{nn}'}(\mathbf{r}) + W_{\text{nn}'}(\mathbf{r})] F_{\text{n}'}(\mathbf{r}) \tag{3.3}$$

where the direct interaction matrix elements are defined by

$$[V_{\text{nn}'} = \langle n / V_{\text{em}} / n' \rangle, \tag{3.4}$$

and the exchange interaction matrix elements, $W_{nn'}$, are operators which interchange bound orbitals in $\phi_n(\mathbf{r})$ with continuum orbitals. All exchange terms decay exponentially in the asymptotic region $r \rightarrow \infty$ in the same manner as the bound orbitals. Thus, exchange effects are characterized as short range. Expanding the function of $F_n(\mathbf{r})$ in terms of the spherical harmonics, the Eq. (3.3) can be reduced to a set of the coupled equations for the radial function. Then the coupled equations can be solved numerically to obtain the scattering amplitude. Once the scattering amplitudes are obtained, the differential cross section and total cross section can be readily calculable from the conventional procedure as,

$$\frac{d\sigma(\theta)}{d\Omega} = (k_n/k_0)|f_{n0}(k_n, k_0)|^2 \tag{3.5}$$

and

$$\sigma_{0\rightarrow n} = (k_n/k_0)\int dk_n |f_{n0}(k_n, k_0)|^2. \tag{3.6}$$

b. Variational Methods. Since a good review for describing details of the methods which belong to this category has recently appeared [73], a brief description of the main features of each procedure will suffice for present purposes. The Kohn variational method and the Schwinger variational method have been known to provide results with reasonable precision and hence are widely employed for electron scattering problems. Rescigno et al. [74] have implemented the Kohn principle for the T-matrix calculation, and applied it to some systems of electron–molecule scattering. For the Schwinger method, McKoy and his colleagues have further developed the method and applied it very extensively to study various electron–molecules scattering processes, with much success [73]. Interested readers are referred to these two review articles for more detailed information.

c. The R-Matrix Method. The R-matrix method was originally suggested by Wigner and colleagues [75] for the study of nuclear reactions and was later adopted by Burke et al. [76–78] for electron scattering problems. This method has been extensively tested and applied for electron–molecule scattering [79,80a], and is now widely believed to offer a reasonably accurate result. The basic concept underlying the method is the division of configuration space into two regions. In the internal region, where complicated, multicenter interactions occur, it is necessary to solve the quantum chemistry problem for the (incoming particle + all target electrons)-system accurately. In the external region, all interactions can be

well approximated by using a single-centered expansion, provided that the asymptotic charge distribution and polarizability of the target are known. The internal region is surrounded by a sphere centered at the molecular center, and two different types of Schrödinger equations from each region separately may be solved and match the solutions at the boundary. Once the internal problem has been solved it is possible to construct the R-matrix on the boundary, which contains information necessary for scattering dynamics. This method has been applied over the past decade to investigate elastic, rovibrational excitation, and electronic excitation processes resulting from electron scattering from atoms and simple molecules, and it has provided much insight into the mechanisms [80b]. Recently the method has begun to be employed to study positron scattering.

d. Continuum Multiple-Scattering (CMS) Method. In a quite different theoretical category from the methods described above, the continuum multiple-scattering (CMS) method is a simple but efficient model for treating electron and positron scattering from polyatomic molecules [81,82]. In order to overcome difficulties arising from, first, the many degrees of freedom of electronic and nuclear motions and, second, the nonspherical molecular field in a polyatomic molecule, the CMS divides the configuration space into three regions: Region I, the atomic region surrounding each atomic sphere (spherical potentials); Region II, the interstitial region (a constant potential); and Region III, the outer region surrounding the molecule (a spherical potential). The scattering part of the method is based on the static-exchange-polarization potential model within the fixed-nuclei approximation. The static interaction is constructed by the electron density based on the present CMS wave function, and the Hara-type free-electron gas model is employed for the local-exchange interaction, while the polarization interaction is considered for only terms proportional to r^{-4}. A simple local exchange potential replaces the cumbersome nonlocal exchange potential, making the practical calculation tractable.

Under these assumptions, the Schrödinger equation in each region is solved numerically under separate boundary conditions. By matching the wave functions and their derivatives from each region, it is possible to determine the total wave functions of the scattered electron and hence also the scattering S-matrix. Once the S-matrix is known, the scattering cross section can be easily calculated. This approach has been employed extensively by Dehmer and his colleagues [83,84] and by Kimura and Sato [85] to successfully provide basic dynamics of elastic and vibrational excitation processes in electron scattering for various molecules. Despite its intrinsic simplicity, it is now, regarded as a useful tool, for providing valuable information on the underlying scattering physics. Further, the CMS

method is useful for guiding the interpolation and extrapolation of experimental data points.

Regardless of the method adopted for solving scattering dynamics from among those described above, the essential aspect of a successful calculation technique depends completely on choosing and constructing accomplishment of realistic interaction potentials between electron, or positron, and the target molecules, which constitutes the most formidable part of theory. Generally, for high energy scattering above a few 10 eV, a dynamical calculation becomes less sensitive to effects of the interaction potentials adopted, and reasonable agreement between theory and experiment for elastic and some inelastic scattering processes can be often achieved. The calculation becomes more and more sensitive to the interaction potentials as the scattering energy decreases to the region of a few eV and below. This is the energy domain that poses a great challenge to theorists as well as experimentalists for detailed investigations. Interaction potentials are here examined in some depth.

B. Electron– and Positron–Molecule Interaction

In order to properly understand and evaluate scattering dynamics, possessing an accurate knowledge of electron– or positron–molecule interactions is essential. In principle, it is not possible to define such interactions unambiguously because some interactions are dynamical in nature, and some relate and interconnect with each other in a complex fashion at certain distances between the incident electron or positron and the target molecule.

However, it is customarily accepted that to arrive at a good approximation it would be helpful to divide the interaction potentials into three parts, namely, static interaction, exchange interaction, and correlation–polarization interaction [73]. The static interaction is the electrostatic interaction between the incident particle and the undeformed target-molecule charge distribution, while the correlation–polarization interaction is the result of electron interaction with the induced dipole moment of the molecule, and both are long-range interactions. The exchange interaction results from the exchange of the incident electron and molecular electrons. In principle, this interaction is nonlocal in nature because it is governed by the overlap of two electron wave functions. Hence, it decays exponentially, and is the short-range interaction.

For positron impact, this latter interaction is completely absent. The correlation–polarization interaction is the result of deformation of the target molecular charge distribution by the approach of an incident electron or positron at large separation. However, when the incident particle comes sufficiently close to the target charge cloud, the incident particle and the

target electrons then correlate strongly with the result that the correlation interaction becomes more complex, making accurate treatment difficult.

The most unique feature of a molecule is the nonspherical anisotropic nature of the potential, and very interesting scattering phenomena and a uniqueness for each molecule emerge as a result of these specific characteristics of the potential. Hence, these features should be carefully built into any theory adopted in as realistical a manner as possible for better description of the collision dynamics. These features, however, pose an extraordinary challenge to theorists in addressing electron– and positron–polyatomic molecule scattering. Furthermore, because of the presence of these features in the potentials even in higher energy regions where the perturbative approach is known to be valid, it is not certain if fully converged results are attainable. Hence, a careful convergence test of the cross section with respect to the potential term should be undertaken.

1. *Static and Correlation–Polarization Interaction*

a. The Static Interaction. The static interaction is given in terms of the charge distribution $\rho(\mathbf{r})$ inside the molecule as

$$V_{\text{static}}(\mathbf{r}) = q\int[\rho(\mathbf{r})/|\mathbf{r}-\mathbf{r}'|]\mathrm{d}\mathbf{r}', \tag{3.7}$$

where q represents the electron or positron charge; for electrons, $q=-e$ and for positrons, $q=+e$. $\mathbf{r}$ is the position vector of the incident electron or positron. The charge distribution $\rho(\mathbf{r})$ includes both the point charges of the nuclei and the molecular electron cloud. If the contribution to the integral from the region $r'>r$ can be safely neglected, then we can expand the term of $1/|\mathbf{r}-\mathbf{r}'|$ and obtain

$$V_{\text{static}}(\mathbf{r}) = q\sum\sum r^{-n-1}Y^{*}_{\text{nm}}(\hat{r})[4\pi/(2n+1)]\times\int\rho(\mathbf{r}')r'^{n}Y_{\text{nm}}(\hat{r}')\mathrm{d}r' \tag{3.8}$$

When the incident particle is far outside the molecule, only the first few terms in the expansion are important, and hence can be expressed as,

$$V_{\text{static}}(r)\rightarrow Zqe/r+(D(R)q/r^{2})P_{1}(\mathbf{R}\cdot\mathbf{r})+(Q(R)q/r^{3})P_{2}(\mathbf{R}\cdot\mathbf{r})+\ldots \tag{3.9}$$

where $P_1(\mathbf{R}\cdot\mathbf{r})$ represents the Legendre polynomial, with R being the internuclear coordinate of the molecule. Note that for a polar molecule, the

dipole interaction, $D(R)$, is important, while for a nonpolar molecule, the quadrupole interaction, $Q(R)$, is the leading term for the interaction, although it is a very weak interaction. These interactions depend on the molecular orientation relative to the direction of the incident electron or positron, and this orientation dependence exerts a torque on the molecule, resulting in a rotational transition of the molecule. In addition, the moments $D(R)$ and $Q(R)$ depend on the internuclear separations within the molecule, and hence, the interaction can also cause a vibrational transition of the molecule.

b. The Correlation–Polarization Interaction for Electrons and Positrons. The correlation–polarization interaction is given by the correlation effect due to the electron or positron interaction with the induced dipole moment of the molecule. When the electron or positron approaches the molecule sufficiently closely, the electric field it produces is no longer uniform over the molecular dimension. Therefore, an asymptotic expansion completely breaks down. There is no unambiguous way to describe the correlation interaction correctly, except for some proposed approximate forms of description on the basis of the localized electron or positron in an electron or positron gas. Knowledge bearing on positron–electron correlation in particular is virtually nonexistent, and hence complete reliance must be placed on a model for purposes of description. In some models, the correlation interaction for electrons and positrons is represented approximately. Examples of the model potentials commonly used for electrons and positrons are shown in the following equations.

For the positron case [86], three forms are used for different r region as

$$2V_{\text{corr}} = (-1.82/\sqrt{r_s}) + \{0.051\ln(r_s) - 0.115\}\ln(r_s) + 1.167 \qquad r_s < 0.302 \tag{3.10}$$

$$2V_{\text{corr}} = -0.92305 - 0.09098/r_s^2 \qquad 0.302 \leqq r_s \leqq 0.56 \tag{3.11}$$

$$2V_{\text{corr}} = -8.7674r_s/(r_s + 2.5)^3 + \{-13.151 + 0.9552\,r_s\}/(r_s + 2.5)^2 + 2.8655/(r_s + 2.5) - 0.6298 \qquad 0.56 \leqq r_s \leqq 8.0 \tag{3.12}$$

Similarly, for the electron case [87],

$$V_{\text{corr}} = 0.0311\ln(r_s) - 0.0584 + 0.006r_s\ln(r_s) - 0.015r_s \qquad r_s \leqq 0.7 \tag{3.13}$$

$$V_{\text{corr}} = -0.07356 + 0.02224\ln(r_s) \qquad 0.7 \leqq r_s \leqq 10.0 \tag{3.14}$$

$$V_{\text{corr}} = -0.584r_s^{-1} + 1.988r_s^{-3/2} - 2.450r_s^{-2} - 0.733r_s^{-5/2} \qquad 10.0 \leqq r_s \tag{3.15}$$

where

$$r_s = [3/\{4\pi\rho^{el}(r)\}]^{1/3} \tag{3.16}$$

If the electron or positron is far from the molecule, the electric field produced by the particle at the molecular site is practically uniform. Then, if the system is spherical, the asymptotic polarization interaction potential is given by

$$V_{pol}(r) \to -\alpha q^2/2r^4 \tag{3.17}$$

where α is the electric dipole polarizability of the target molecule. V_{corr} and V_{pol} join smoothly at intermediate r (normally, 8–10 a_0) to represent both short- and long-range parts of the interaction uniformly.

For most molecules, the polarizability is a tensor property, depending on the orientation of the molecule relative to the applied electric field. For linear molecules, for instance, the polarizability is expected to be generally larger along the molecular axis than in the perpendicular direction, because more space is available for the molecular electrons and hence they can move more freely along the axis than in the perpendicular directions. It should be noted that the polarizability also depends upon the nature of the molecular bond and electron charge distribution. For the linear molecule case, the asymptotic potential is replaced by

$$V_{pol}(\mathbf{R}, \mathbf{r}) \to -\alpha q^2/2r^4 - (\alpha' q^2/2r^4)P_2(\mathbf{R} \cdot \mathbf{r}), \tag{3.18}$$

where α and α' are given by the polarizabilities along the directions parallel ($\alpha_\parallel$) and perpendicular ($\alpha_\perp$) to the molecular axis R in the form,

$$\alpha = (\alpha_\parallel + 2\alpha_\perp)/3 \tag{3.19}$$

and

$$\alpha = (2/3)(\alpha_\parallel - \alpha_\perp). \tag{3.20}$$

To make this polarization potential more complicated, there is a velocity dependence in the polarization interaction. When the incident electron or positron velocity is small, the collision time is long, and hence, the molecular electron cloud can adjust to the motion of the incoming electron or positron adiabatically. Then the adiabatic polarization potential, given by Eqs. (3.10–3.12) or (3.14) and (3.15), and (3.18), can be used with reasonable accuracy for describing the polarization effect. When the incident electron or positron velocity becomes higher, the collision duration

becomes shorter and hence the molecular electron cloud cannot be adiabatically deformed. Therefore, the polarization interaction is expected to become less important as the collision velocity becomes higher. Such a velocity dependence of the polarization interaction needs to be correctly taken into account in principle. In reality, however, it produces a formidable task for theorists, and up to this writing (ca. a 1999) a rigorous treatment has not been established, except for some model interactions [88].

2. *Exchange Interactions*

The exchange effect arises from antisymmetrization of the wave function of the whole system with respect to the electrons, including the incident electron and hence is a unique feature of electron impact. It leads to a set of coupled integrodifferential equations rather than a set of coupled differential equations. Therefore, the exchange effect gives rise to a nonlocal interaction. In order to simplify the exchange interaction, the nonlocal exchange interaction is often replaced by an appropriate and simpler local potential. Here the exact nonlocal exchange interaction can be written in terms of the one-electron wave function, $\phi(\mathbf{r})$, of a bound electron and the incident single-electron wave function, $\psi(\mathbf{r})$, as,

$$V_{\text{exch}}(\mathbf{r}) = -\sum \phi(\mathbf{r}) \int \phi^*(\mathbf{r}')[q^2/|\mathbf{r}-\mathbf{r}'|]\psi(\mathbf{r}')\mathrm{d}\mathbf{r}'. \tag{3.21}$$

This nonlocal expression can be replaced by an approximate local-exchange potential,

$$V_{\text{exch}}(\mathbf{r}) = \left[-\sum \int \phi^*(\mathbf{r}')\psi^*(\mathbf{r})\{q^2/|\mathbf{r}-\mathbf{r}'|\}\phi(\mathbf{r})\psi(\mathbf{r}')\mathrm{d}\mathbf{r}'\right] \Big/ \psi(\mathbf{r})^2. \tag{3.22}$$

Slater [89] derived a more realistic and tractable form of the exchange interaction by limiting the integration area within a certain boundary, as follows:

$$V_{\text{exch}} \cong [q^2/2\pi^2] \int \mathrm{d}\mathbf{k}'/|\mathbf{k}'-\mathbf{k}|^2 \tag{3.23}$$

The integral is taken over the region of k' occupied by the orbital electrons. By taking the average over the relative orientation of k and k', the integration can be carried out as

$$\int \mathrm{d}k'/(k'-k) = [2\pi/(k'k)]\ln[(k'+k)/(k'-k)] \tag{3.24}$$

For collisions of $k > k'$ (which is always the case), by integrating over k, one obtains

$$V_{\text{exch}} = -[q^2/\pi]k_{\max}\{1 - [(k^2 - k_{\max}^2)/(2kk_{\max})]\ln[(k + k_{\max})/(k - k_{\max})]\}. \tag{3.25}$$

where $k_{\max}(r)$ is the maximum wave number in the local bound electron distribution, and is given by

$$k_{\max}(r) = (3\pi^2 n_e)^{1/3} \tag{3.26}$$

where n_e is the local bound-electron density.

The incident electron wave number k_0 relates to the ionization potential, I, of the target molecule and $k_{\max}$ within the local approximation as

$$\hbar^2 k(r)^2/2m_e = \hbar^2 k_0^2/2m_e + \hbar^2 k_{\max}^2/2m_e + \text{I}, \tag{3.27}$$

Eq. (3.25), as well as Eqs. (3.26) (3.27), are now in a local exchange model, often termed the Hara-exchange interaction potential [90]. This exchange interaction, along with other, similar forms, has frequently been utilized for electron scattering as a standard exchange model. Whether this exchange interaction is attractive or repulsive depends on the initial electronic state of the molecule, and for the ground electronic state it is generally believed to be attractive. For excited electronic states, no comprehensive study exists.

For clear visualization, the spherical part of the interaction potentials arising from the three terms, i.e., the static, exchange and correlation-polarization interactions, above are plotted in Figure 11(a) and (b), respectively, for the positron and electron interactions with the CH_4 molecule as a function of electron– or positron–molecule distance [91]. For the electron interaction, the static, correlation–polarization, and exchange interactions are all attractive and hence the total interaction is the sum of all three contributions, while for positron interaction, the static interaction and correlation–polarization interaction have a different sign and hence they cancel each other. Therefore, as seen for positrons, at smaller r within about 1.4 a_0, the total interaction becomes strongly repulsive because the static interaction dominates, while at larger r beyond 1.4 a_0, it becomes attractive because of the polarization interaction. In the region in between, one can observe a shallow well around 3.2 a_0, and this type of well may be able to hold the incoming positron temporarily, causing a resonance state, i.e., positron-in-molecule. This resonance may be significant in lending support for the dynamical point of view, as discussed in a later Section IV.E. Figure 11(b) clearly demonstrates that the total interaction for the electron is

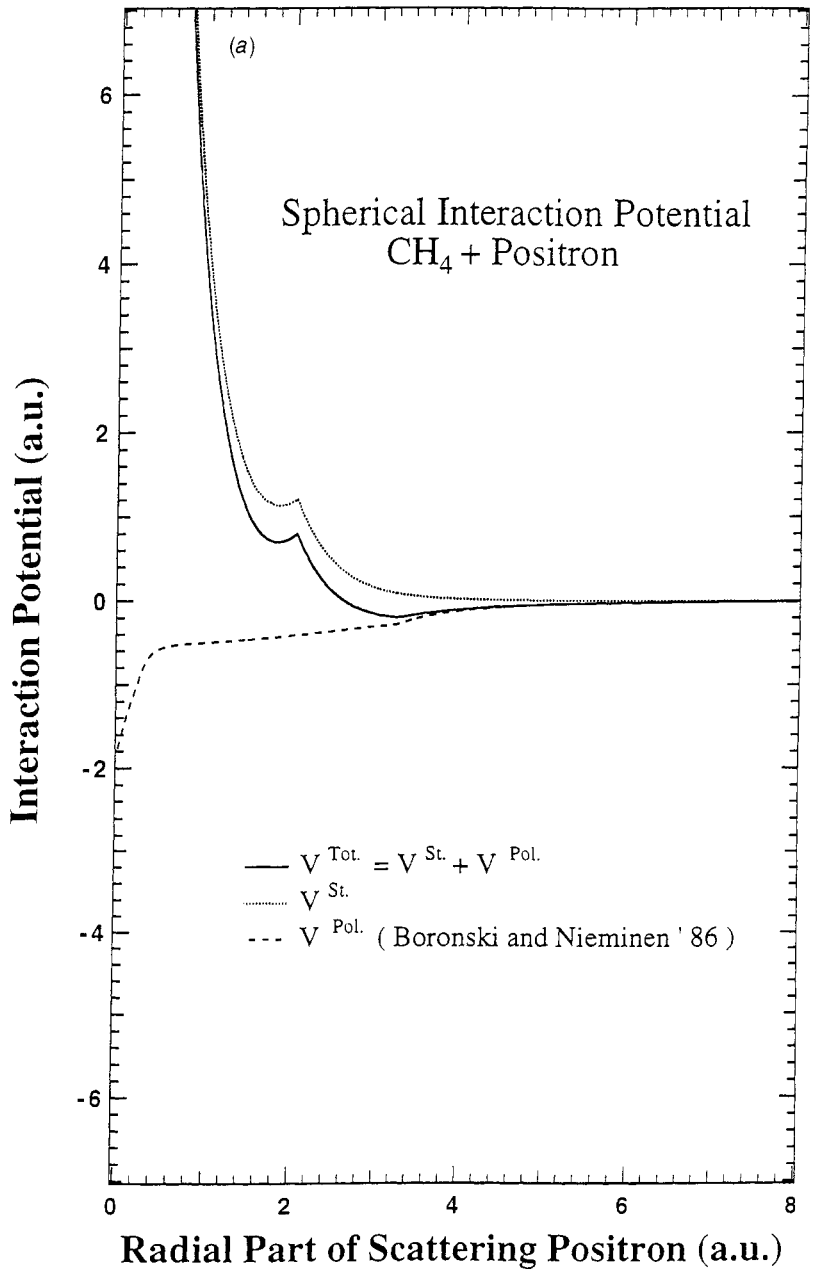

FIGURE 11. Interaction potentials for (*a*) e^+–CH_4 and (*b*) e^-–CH_4 (a spherical part only). The total (sum) (*solid line*) of all interactions and each contribution is also included.

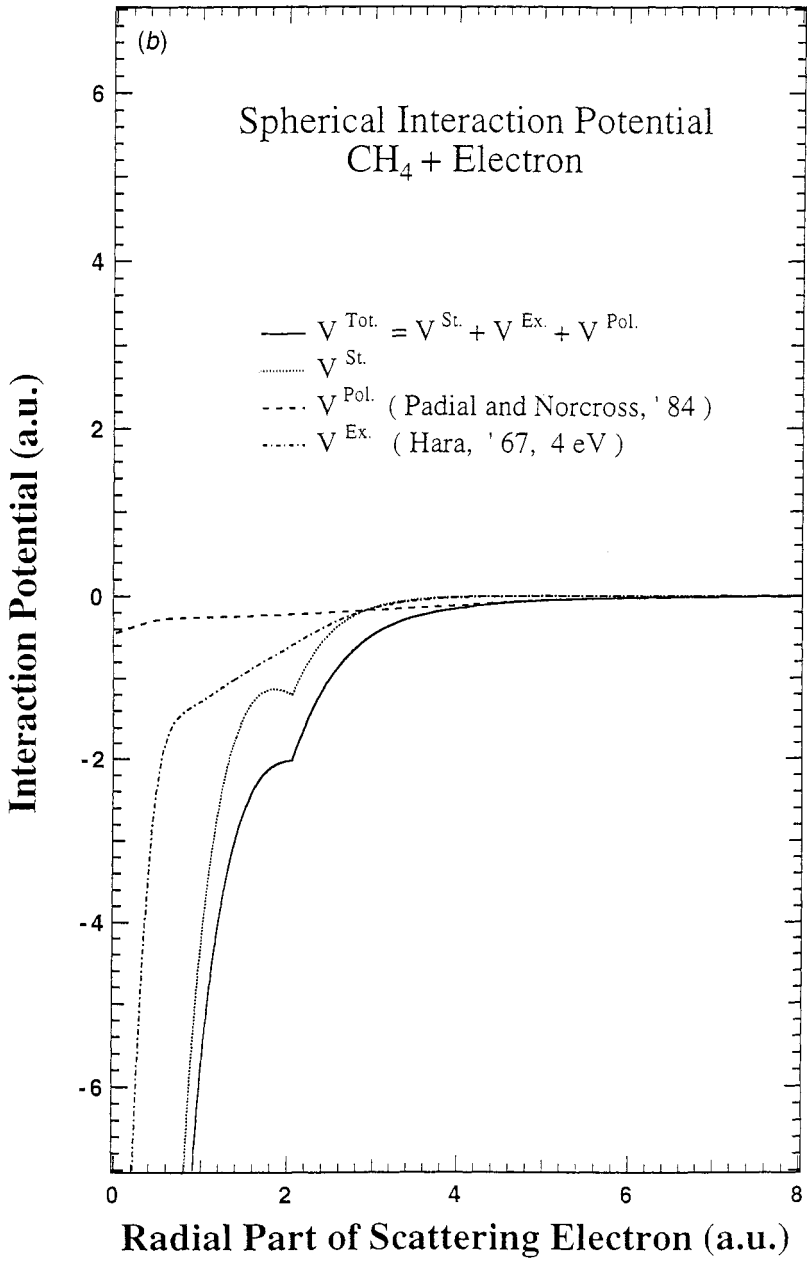

FIGURE 11. (*Continued*)

uniformly attractive. The kink seen at 2.05 a_0 is due to the charge distribution from the H nucleus in methane. At much larger r, the total interaction is primarily governed by the polarization, and eventually becomes the polarization potential itself in the asymptotic region. In general, because of the cancellation of the interaction for positrons, the total interaction becomes highly sensitive to the choice of the polarization potential because it controls the point where the total interaction changes its character from attractive to repulsive and hence also the slope of the potential. These factors, in turn, reflect on scattering calculation, making high-precision positron scattering calculations more difficult to achieve, as exemplified in the figures.

The above argument is based on the spherical part of the interaction potential, and hence holds only for the the s-wave scattering. In reality, the electron and positron interaction potential is essentially nonspherical, and instead has a more complicated form of which it is not easy to make a simple illustration.

It is appropriate here to summarize the effect of each contribution of the interaction potential given in Table IV and already discussed at some length. For electron impact, the static and correlation–polarization interactions have the same sign, and therefore they add up, causing stronger interactions. The additional effect from the exchange interaction is short-range, and with this exchange interaction, the sum of three interactions behaves in a complex manner. For positron impact, the static interaction and correlation–polarization interactions have a different sign, and hence they subtract each other, weakening the overall interaction. Of course, as described above, there is no contribution from the exchange interaction for positrons. The cancellation introduces a weak attractive well in the spherical component outside the charge cloud of the molecule, as seen above. The depth and shape of this well profoundly influence scattering and hence, how the polarization is included is critical as positron–molecule scattering calculations become highly sensitive to the approximations employed in the treatment of polarization. Furthermore, this attractive well might hold the incoming positron, resulting in the possibility of a resonance similar to

TABLE IV
Electron and Positron Interactions

Type	e^-	e^+
Static	attractive	repulsive
Polarization	attractive	attractive
Exchange	attractive	—
Sum	addition	cancel

shape resonances in electron scattering. Also, the situation becomes more and more favorable for the resonance formation if the molecular size and hence the number of electrons in a molecule increases owing to a more complex potential structure. This subject is discussed in greater detail and specific cases are extensively treated below.

Some conspicuous effects and consequences resulting from the differing nature of the interaction potential to which electrons and positrons are respectively subjected may be listed at the outset of a more detailed discussion, which follows. They are

1. New appearance of the Ramsauer–Townsend (RT) effect in the elastic cross section for positron scattering from H and He atoms and some molecules
2. Direct annihilation of a positron through its interaction with electrons in atoms and molecules
3. New types of resonances
4. An effect of charge transfer to the continuum on the part of the ionization process

C. Positronium Formation

Positronium formation is a unique feature observed in most instances of positron scattering, and it has stimulated a great deal of experimental and theoretical work geared to accurately determining the positronium formation fraction during the slowing-down process in a high-density noble gas. Despite many experimental attempts, very few accurate measurements of absolute cross sections for positronium formation from atomic and molecular targets had earlier been reported. Only recently has significant progress been made, and very interesting measurements are now being performed at Wayne State University. For the positronium formation to be possible, the incident positron energy should satisfy the relationship,

$$E \geqq (E_I - 6.8)\text{eV}, \tag{3.28}$$

where E and E_I are the incident energy of the positron, and the ionization energy of a target molecule, respectively [92], and the equal sign corresponds to the threshold of positronium formation. For normal atoms and molecules, the threshold of positronium formation is roughly in the 6–8 eV region, and an electronic excitation channel opens almost in the same energy region. Therefore, thresholds for these two channels nearly overlap and hence are expected to interfere with each other, causing structures in TCS or DCS. In the immediate vicinity of the threshold for Ps-

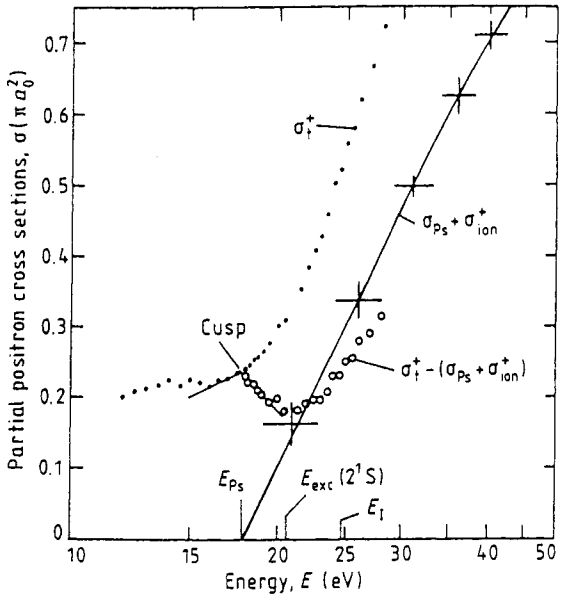

FIGURE 12. An example of the Wigner cusp resulting from positron impact on He. From Ref. [62].

formation, the Ps-formation cross section can be written in the power-law form of the lowest partial wave contribution as,

$$\sigma_{Ps}(E) \sim (E - E_{Ps})^{1/2} \tag{3.29}$$

This form has been fitted to various data, and has led to the first experimental evidence of a threshold anomaly (Wigner cusp) in the elastic cross section for He and H_2 [48]. An example of the Wigner cusp is illustrated in Figure 12, which shows the data for the He obtained by the Bielefeld group (1987) [62].

Alternatively, this process may be regarded as equivalent to charge transfer or electron capture in ion–atom collisions. If an electron from the target fails to be captured by an incoming positron, then it ends up as part of an ionization event or, in ion–atom terminology, as a charge transfer-to-continuum [93]. Therefore, sometimes the ionization cross section caused by positron impact is found to be larger than that of electron impact (a good example of this is seen in the He target). This is the case because for positrons, ionization is a sum of direct impact ionization and charge-transfer to the continuum, while for electron impact, only direct impact ionization is

possible, making the cross section somewhat smaller than the positron counterpart.

To substantiate this argument using the analogy of charge transfer, a collision system of proton impact on an atomic target may be considered. For the proton impact, usually a maximum in charge-transfer cross sections occurs near the velocity where that of an orbital (transferred) electron nearly matches that of the incident particle (velocity-matching condition). For an $H^+ + H$ collision system, for example, the orbital velocity of $H(1s)$ electron is 1 a.u., and hence, the charge-transfer cross section to $H(n=2)$ levels must have a peak when the incident proton has roughly the incident energy of 25keV/u (or 1 a.u. in proton velocity), which has been experimentally confirmed [94]. For positronium formation, as will be shown below, positronium formation cross sections available from experiments generally appear to show a maximum in the neighborhood of 27–30 eV, which is consistent with the ion–atom collision case, and indeed the positronium formation can be regarded as equivalent to charge transfer.

D. Weak Interaction Approximation

When the incident particle passes by far outside the target, or its velocity is so fast that the interaction time between the projectile and target is very short, then the interaction is considered to be weak. For such a case, the coupled equation in Eq. (3.3) can be solved by using perturbation methods. The Born approximation is the simplest of all approximations and it can provide a simple picture of collision dynamics. Rotational excitation and, to a lesser extent, vibrational excitation by electron or positron impact with near-threshold energies can be induced by the weak long-range interaction, and therefore the Born treatment may be appropriate. For rotational and vibrational (rovibrational) excitation processes, the asymptotic interaction between electron, or positron, and the target molecule can be represented as

$$\begin{aligned} V(r) \to & -\alpha e^2/2r^4 \mp [D(R)e/r^2]P_1(R\cdot r) \\ & -[\alpha e^2/2r^4 \pm Q(R)e/r^3]P_2(R\cdot r) + \cdots \end{aligned} \tag{3.30}$$

where the upper sign represents the electron, and the lower sign the positron. Then the excitation cross section for this interaction based on the Born approximation for a non-polar molecule [95] is given as

$$\sigma \sim f(k_i, k_f, v, J)[Q(r)^2 \pm Q(r)\alpha(r)g(k_i, k_f) + \alpha(r)^2 h(k_i, k_f)], \tag{3.31}$$

where, again, the upper sign is for electron and lower sign is for positron, and $Q(R)$ and $\alpha(R)$ represent quadrupole moment and polarizability,

respectively. The expression $f(k_i.k_f, v, J)$ $g(k_i, k_f)$ and $h(k_i, k_f)$ are functions of initial and final momenta (k_i and k_f) and rovibrational quantum number (v, J) only. For rotational excitation, $Q(R)$ and $\alpha(R)$ are simply the quadrupole moment and polarizability. Therefore, it is clear that if a target molecule has a negative quadrupole moment, then rotational excitation cross section for positron impact should become larger than that of electron impact, at least near the threshold region. This finding based on the Born approximation shown in Eq. (3.31) was first indicated by Takayanagi and Inokuti for a molecule with the negative $Q(R)$ value such as the N_2 [1]. For vibrational excitation, these Q and α are sandwiched by nuclear wave functions to form the matrix element, i.e., $\langle v'/Q(R)/v\rangle$. For the much lower excited vibrational states, this matrix element can be reduced to a simpler form, $\sim \mathrm{d}Q(R)/\mathrm{d}R\langle v'|(R\text{–}R_{\mathrm{eq}})|v\rangle$. From Eq. (3.31), the vibrational excitation cross section for positron impact, like that for rotational excitation, should also be larger than that for electron impact only if the derivative of the quadrupole moment is negative. However, a close comparative study between the close–coupling method and the Born approach shows rather poor agreement between the two methods [96], and hence the validity of the Born approximation is less clear for the vibrational excitation, and a certain amount of care must be taken when this approach is used.

For momentum-transfer processes for molecules with a permanent dipole moment, based on the Born argument with the contribution from the long-range interaction, the cross sections in the low energy range (below ~ 0.1 eV) are known to be represented by the simple form as

$$\sigma_{\mathrm{tot}} \sim (f(D)/v^2) \tag{3.32}$$

where $f(D)$ is a function of the dipole moment, D, of the molecule and v is the speed of the electron or positron. Eq. (3.32) suggests that the momentum- transfer cross section increases as the inverse of the collision energy for polar-molecule cases as the energy is lowered. For nonpolar molecules, similar simple forms for describing the momentum-transfer process have been proposed but are still the subject of debate. For total and elastic cross sections, because of the divergence arising from the dipole interaction, simple forms similar to Eq. (3.32) are not known, but that is consistent with the fact that they are much more complicated [97].

The scattering length theory at the limit of zero scattering energy is known to provide useful information on the elastic cross section in a limiting case [98]. For molecules such as CO_2, the elastic cross section caused by electron impact is known to increase as the energy decreases, being similar in its behavior to a polar molecule, due to the s-wave resonance (virtual state) at the threshold [99]. Most of the others seem to

flatten and approach a constant value, or to decrease toward the zero energy forming an area in which swarm-type experiments have been aiming at exploring details of the dynamics as well as the cross-section values [100]. The information derived from the scattering length theory also serves well for these purposes.

E. Resonance

Resonances for electron scattering have been known for some time and have been a subject of both experimental and theoretical studies; a great deal of knowledge of their dynamics and nature has thus been accumulated. In contrast to the situation obtained for electron scattering, very little is known about resonance for positron scattering, although its existence has been predicted for some time [101], and a few experimental attempts based on annihilation of positrons have been performed to search for the basis of the existence of the resonances. Earlier experiments by Paul and Saint-Pierre [102] found a large annihilation rate as the molecular size becomes larger, indicating a possible bound state of the positron in a molecule. In recent experiments, some more direct evidence of resonances has reportedly been observed, or actually claimed to have been confirmed [64,103–105]. Although a thorough analysis of these findings is still lacking, some general comments on this new phenomenon are perhaps warranted.

Resonances introduce conspicuous features in cross sections for various processes and have various important consequences. Resonance as such is the temporary formation of a compound state between the incident electron and the target molecule with a lifetime appreciably longer than the electron passage time, a/v (a being the linear dimension of the target molecule and v the incident electron velocity). At some incident energy, the electron wave function has a large amplitude within the target. This is possible only when the incident energy falls in one of the discrete bands, where the incident electron finds a comfortable quasistationary orbit in the field of the target molecule. The quasistationary nature of the compound state is usually considered to be possible by virtue of either of the following two mechanisms. The first possibility is the existence of an appreciable barrier in the effective potential (attractive polarization force plus the centrifugal force). Once the electron has entered the region inside the barrier, it will take some time before the electron emerges into the outer region through the tunneling effect. The resonance caused through this mechanism is often called shape resonance, since it depends sensitively on the shape of the potential which the incident electron "feels". The second possibility arises when the inelastic channels are introduced. By exciting the target molecule, the electron loses its energy, having then a negative energy which coincides with one of the bound state energies. Then it takes

some time before the electron recovers its energy and moves out of the molecular field. The resonance from this second mechanism is called Feshbach resonance.

For positron impact, the two types of resonances are both possible. Furthermore, there are two additional possibilities of resonance arising. First, coupled channel shape resonance, based on theoretical prediction by Higgins and Burke [106] for positron–H elastic scattering, occurs as result of the coupling between Ps formation and elastic channels at intermediate energy, (around 40–50 eV). Kauppila's group [12] has first claimed to have observed this resonance experimentally in their DCS for positron–rare gas (Ar, Kr) atom scattering at 55–60 eV. (However, more recent their measurements were unable to reproduce their initial results [107].) Second, when the incident positron comes close to the molecular electron charge cloud, the cloud deforms toward the incoming positron through electron–positron attractive correlation, thus "wrapping up" and holding the positron to form a temporary bound state, positronium-in-molecule; this occurrence is possible at low energy, below a few eV. The excess energy arising from the positron kinetic energy plus the positron-affinity for the molecule can be dissipated and shared by many rovibrational modes of the molecule. Since the more the molecular size increases, the more these levels become available, polyatomic molecules offer a better chance for trapping the positron. This resonance state will decay either through the escape of the positron or through annihilation followed by the γ-ray emission. However, this resonance state is expected to be a short-lived state with a broad structure in total cross section below the scattering energy of 1 eV, and if the number of electrons in the target increases (i.e., in the case of larger polyatomic molecules), this phenomenon should be more likely to occur [103]. This mechanism may be viewed as a type of shape resonance since the positron is trapped by the attractive potential created by the molecular electron charge distribution, as discussed as an example of the potential in the Section III.B.

IV. EXPERIMENTAL RESULTS AND ANALYSIS

In electron and positron scattering from molecules, elastic as well as a few inelastic processes are possible, and among those, ionization ($> \sim 10$–15 eV), electronic excitation (~ 4–9 eV), and rovibrational excitation (< 0.2 eV) are known to take place for both projectiles with large values of the cross sections. There are a few interesting features in cross sections for each channel: some are very strong in a certain impact energy region, while others dominate in other energy regions. Some may compete with

others in overlapping energy regions. Electron attachment is known to exist for electron impact below a few eV and in fact, for some cases a molecular dissociation readily proceeds through this channel. Positron attachment has not yet been directly observed experimentally, but this process is firmly believed to exist, on the basis of indirect evidence. However, as discussed in Section III.E above, this process may be possible through a shallow attractive well of the potential (which large polyatomic molecules can readily generate) and may provide significant consequences for the parent molecule to dissociate, and be the subject of rovibrational excitation. This positron attachment may end in annihilation of the positron, leaving behind molecular ions. These molecular ions are significant for various applications because they are formed in a nonviolent manner and hence can have a long lifetime before undergoing fragmentation. Furthermore, these ions can be useful from the spectroscopic and molecular structural-determination points of view. Indeed recently, Ryzhikh and Mitroy [23] have suggested theoretically that a positron can attach to a Li-containing molecule. In addition, positronium formation is a unique process in which its threshold is close to electronic excitation and ionization, as given in Eq. (3.28). Therefore, for positrons, within a narrow energy range from ~ 4–15 eV, Ps-formation, electronic excitation and impact ionization processes occur, and hence these processes cause the formation of a series of structures in the total cross section. Some channels are expected to interfere or couple with weaker channels like the elastic process, resulting in additional structures. One good example may be the Wigner cusp.

As described in Section II.A earlier, at present, detailed experimental measurements for each process for positron scattering are nearly nonexistent. The only exceptions are very exploratory studies on rovibrational excitation for very limited molecules, and in terms of positronium formation, mostly for rare gases and alkali atoms. Most of the experimental activities at present concentrate on measurements of total (a sum of all elastic and inelastic processes) and, to lesser extent, differential cross sections. Hence, some very interesting and prominent features seen separately in total cross sections for a number of different groups of molecules in relation to one another are discussed first. Then each inelastic process is discussed to some degree, although very little information for inelastic processes from either experiment or theory is available, and in fact, for some processes it is completely absent. Whether a molecule possesses a permanent dipole moment or not makes a huge qualitative and quantitative difference to dynamical aspects, particularly at the lower range of incident energy, and this may therefore be a good parameter by which to classify molecules into small groups. For reference, the molecules we have studied according to this classification are shown in Table V.

TABLE V
Molecules Studied for Total and Ps Formation Cross Sections for This Article

Polar	Nonpolar
CO	CO_2
COS	CH_4, CF_4
HCl	O_2, N_2
H_2O	C_2H_2
NH_3	C_2H_4
CHF_3	C_2H_6, C_2F_6
CH_2F_2	SF_6
C_3H_8, C_3F_8	C_6H_6
C_4H_8, C_4F_8	
CH_3OH	
C_2H_5OH	
HCOOH	
CH_3COOH	
$(CH_3)_2CO$	
$C_6H_5CH_3$	
C_5H_{12}	
C_6H_{12}	
C_8H_{18}	
C_8H_{16}	

As stated above, very little information for any specific inelastic process is available to date, and therefore, some of the discussions of the processes herein may be partly based on circumstantial evidence and thus tend to be speculative. Nevertheless, the various arguments and discussion are given in the hope that they may invite wide open debate of the subject, leading to their replacement in the near future by more rigorous qualitative and quantitative arguments based firmly on experimental or theoretical investigations of other researchers.

A. Total Cross Section

In this section a comparative study of electron and positron impacts on larger molecules is presented, highlighting both the similarity and difference between the two in order to provide the underlying physics and sufficient insight to formulate a general principle of dynamics for molecules[2]. An earlier excellent review article by Kauppila and Stein [14] mainly discussed

[2] Most experimental TCSs presented here have been measured specifically for presentation in this article, and more detailed discussions for each molecular group will be found in forthcoming separate papers. Also, it should be noted that differential cross sections used for the forward scattering correction of positron TCSs were adopted from electron scattering data.

the results for atomic targets, with inclusion of some molecules (H_2, N_2, CO, O_2, H_2O, CO_2, N_2O, NH_3, CH_4, SiH_4, CF_4, and SF_6) from the experimental point of view. That review should be consulted for details of the study of atoms and of those molecules.

Discussion here begins with groups of small molecules covering a range from strong polar molecules to weak polar and nonpolar molecules, and then moves on to hydrocarbons of medium size with or without dipole moment. Then the much larger molecules of hydrocarbons, i.e., those having OH- and COOH-bases, and benzene rings with a mixture of polar and nonpolar molecules are dealt with. In the course of the discussion, general features are given for both of the projectiles, but with an emphasis on unique features specific to individual projectiles.

1. Small Molecules

a. Strong polar molecules: H_2O, NH_3, and HCl. Water, ammonia, and hydrochloric acid molecules have the strongest dipole moment among those studied by us. TCSs by both electron and positron impacts are displayed in Figures 13, and 14 for H_2O and HCl, respectively [39,107–108].

The sharply increasing trend of the TCSs for both the projectiles at lower energies is a clear manifestation of the dipole effect. They also drop sharply

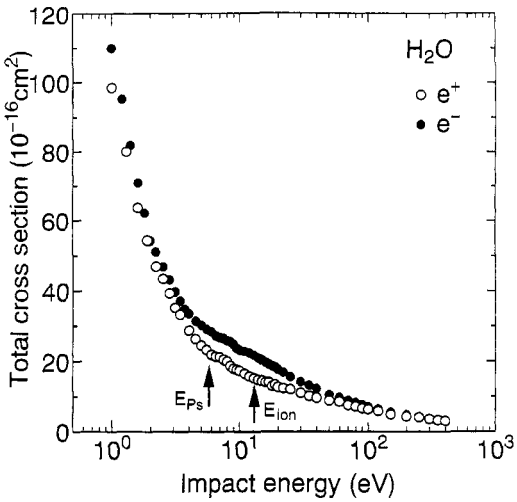

FIGURE 13. TCSs for electron and positron impact on H_2O. Solid circles, ●, are electron impact data by Sueoka and colleagues, and open circles, ○, are those of positron impact by Sueoka and colleagues. Note that thresholds for Ps formation and ionization are indicated by arrows, respectively.

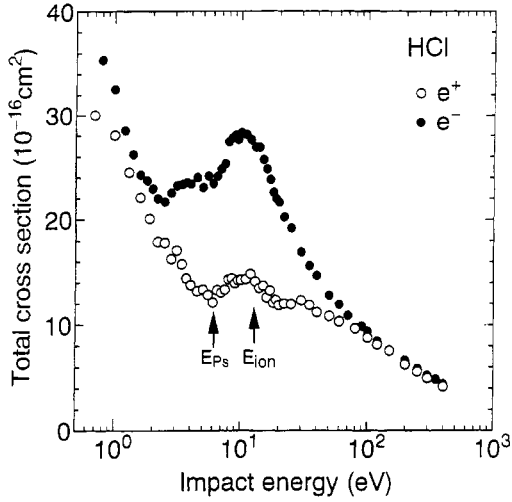

FIGURE 14. TCSs for electron and positron impact on HCl. Solid circles, ●, are electron impact data by Sueoka and colleagues, and open circles, ○, are those of positron impact by Sueoka and colleagues. Note that thresholds for Ps formation and ionization are indicated by arrows, respectively.

as the incident energy increases, and above 100 eV the TCSs for electrons and positrons merge for all the molecules. Below 100 eV, however, TCS for electron, is generally larger in magnitude at intermediate energies because of the weaker interaction for positrons. For NH_3, the magnitude of the TCS for electron and positron reverses at around 2 eV, i.e., the TCS for the positron becomes larger. A similar trend for some molecular systems will be seen, as described below, and this phenomenon is very interesting from the stand point of its considering the contribution of inelastic channels. Detailed discussion of this phenomenon is given later in this section. It is important to mention that the two TCSs for electrons and positrons for H_2O and NH_3 molecules have very little structure except for a small shoulder for electron impact around 10 eV. This shoulder is due primarily to a combination of the shape resonance and the onset of an ionization channel, though it is very weak both for H_2O and NH_3 owing to the dipole effect. Any instance of a similar shoulder is missing in the positron TCSs. Furthermore, the difference between the TCS for electron and that for positron is much smaller than that existing among other molecular systems examined below, which sometimes show a difference by an order of magnitude. These features of the close magnitude of electron and positron TCSs and the lack of structure should owe much to a strong dipole moment. The dipole coupling which is the dominant driving force for inelastic transitions is a long-range one, and

regardless of whether the projectiles can penetrate close to the nucleus or not, it would make little difference in a product of the coupling matrix element and continuum wave function of the incident particle (a significant term to solve in the coupled equation) causing the similarity of the two sets of the TCSs.

The TCS for HCl is different from that of the two molecules above, in some respects. It shows a stronger shape resonance at 10 eV for electron scattering, and the magnitude of the overall TCS is the smallest among the three. As noted above both for H_2O and NH_3, these molecules display only a trace of the resonance in the same energy region. It is also interesting to note that the TCS for positron for HCl shows a similar but weaker structure at around the same energy, which may well be due to the combination of the positronium formation, electronic excitation, and ionization channels. Other than these features, all three molecules show surprisingly similar characteristics in the TCSs at low and high energy regions.

Okamoto et al. [41] have carried out theoretical investigations of a vibrationally elastic cross section for H_2O by electron impact below 50 eV based on the close-coupling method. Their results are in excellent agreement with the TCS measurement of Sueoka et al. [107] as well as DCSs at a few energy points. Jain et al. [109] have studied TCS and DCS for both H_2O and NH_3 molecules by electron and positron impacts by using the optical potential method. Their TCSs are also rather smooth and sharply decrease with the incident energy, qualitatively in good agreement with the measurement.

b. Weak polar and nonpolar molecules. The group of molecules having a weak dipole moment, or nondipole moment and a small molecular size, among those studied were CO, OSC, CO_2. The TCSs for CO, CO_2, and OCS are shown in Figures 15, 16, and 17, respectively, along with the data by the Detroit group.

For TCSs by electron impact, the large peak at 1.8 eV for CO and, to a somewhat lesser extent, that at 1.3 eV for OCS are each due to a $^1\Pi$ shape resonance. The second broad peak, seen around 15–25 eV for CO and 9–20 eV for OCS, is the combination of π_u, π_g, δ_u, δ_g, and other higher partial channels. At energies below 1 eV, which the present measurement method cannot access, the TCSs are expected to increase rather sharply, which is a typical characteristic of a polar molecule as seen in the previous examples. It is interesting to note that the TCS for OCS by electron impact is quite similar to that of CO_2 with respect to the positions of resonances and general features. The same number of valence electrons and analogous molecular structure may be responsible for these similarities, even though OCS is a weak polar molecule and CO_2 a nonpolar molecule. The TCSs by positron

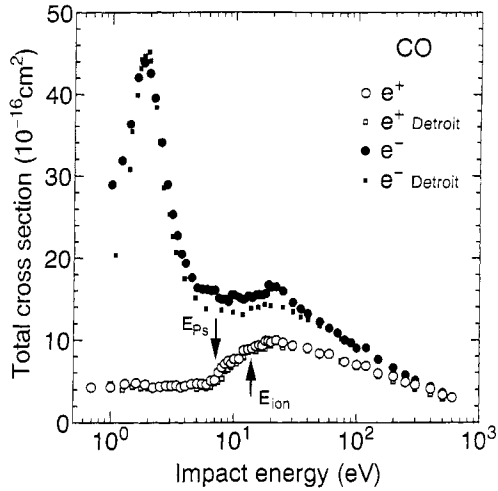

FIGURE 15. TCSs for electron and positron impact on CO. Solid circles, ●, are electron impact data by Sueoka and colleagues, and open circles, ○, are those of positron impact by Sueoka and colleagues ■ are electron-impact TCS data by the Detroit group (Kauppila and Stein's group), and □ are those for positron impact by the Detroit group (Kauppila and Stein's group). Note that thresholds for Ps formation and ionization are indicated by arrows, respectively.

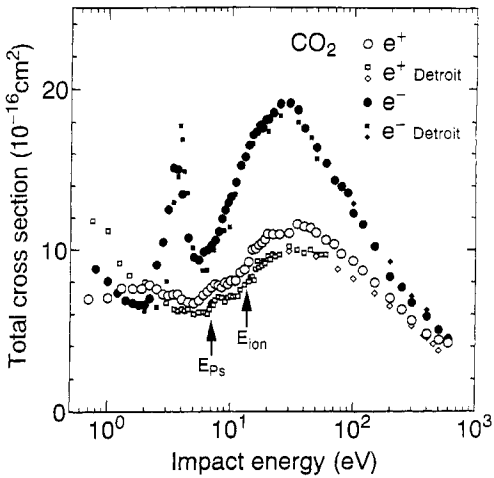

FIGURE 16. TCSs for electron and positron impact on CO_2. Solid circles, ●, are electron impact data by Sueoka and colleagues, and open circles, ○, are those of positron impact by Sueoka and colleagues. ■ are electron-impact TCS data by the Detroit group (Kauppila and Stein's group), and □ are those for positron impact by the Detroit group (Kauppila and Stein's group). Thesholds for Ps formation and ionization are indicated by arrows, respectively.

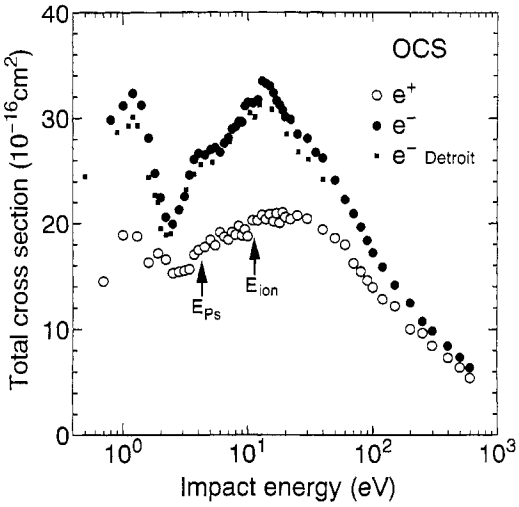

FIGURE 17. TCSs for electron and positron impact on OCS. Solid circles, ●, are electron impact data by Sueoka and colleagues, and open circles, ○, are those of positron impact by Sueoka and colleagues. ■ are electron-impact TCS data by the Detroit group (Kauppila and Stein's group). Thesholds for Ps formation and ionization are indicated by arrows, respectively.

impact have weaker and fewer structures than those of electron impact. An exception is the two humps at 5–7 eV and at slightly above 10 eV, which are due respectively to positronium formation and to a combination of electronic excitation and direct ionization. Both the cross sections for OCS and CO by positron scattering are smaller than those of electron impact at intermediate energies, but quickly merge to the electron TCSs beyond 100 eV. For both the systems, there is no reverse of the TCS in the low energy region as was seen for NH_3. However, as will be seen below, the reverse of the cross sections for electron and positron is observed to take place for CO_2 at 0.8–2 eV, which may be attributable to larger rotational cross sections for positron impact.

Jain and Thompson [110] have carried out a theoretical study for total as well as rovibrational excitation cross sections of CO by electron and positron impact, and have predicted a large disparity of nearly an order of magnitude between the TCSs for electrons and positrons in the 0.5–3 eV region. The positron TCSs are far smaller than those of the electron impact. The ratio of the TCS for positron to that for electron reaches as low as 0.05 at 2 eV, which is consistent with the present experimental ratio. The CMS method was applied to investigate the electron scattering from OCS by Lynch et al. [111]. The general feature observed by experiment was

reproduced reasonably well by the calculation, particularly for the positions of shape resonances and their origins.

The CO_2 molecule is a non-polar triatomic molecule and has been one of the most popular targets for experimental as well as theoretical investigations for electron impact for many years, because of its importance in various applications and its rather well-studied molecular structure. Hence, a reasonable amount of information for elastic and inelastic scattering processes has been accumulated, and a comprehensive data set for these processes is now readily available [100]. However, there still remain some discrepancies in all channels.

As a general feature, the TCS and vibrational excitation cross section by electron impact are known to present a strong resonance-peak at 3.8 eV and a broad resonance around 20–40 eV region, both of which are due to shape resonances. Below the 3.8 eV resonance, the TCS rapidly increases as the scattering energy approaches zero, and this phenomenon is characterized as the existence of a virtual state or strong s-wave resonance at zero energy [72]. The references are too numerous to cite all theoretical attempts, particularly for elastic scattering. (For the most recent studies, see Refs. [21] and [112–114], and references cited in these papers). Some are reasonably successful in obtaining the positions and magnitude of the resonances and reproducing the general shape of the TCS as well as the elastic cross section by employing several types of polarization potential with or without adjustable parameters within a close-coupling scheme. Generally, theory works poorly at low energies because of the difficulty of accurately describing the correlation–polarization interaction, which becomes increasingly important as the energy is lowered. For higher energies above a few 10 eV to a few 100 eV, the agreement between theory and experiment is found to improve without any further adjustment of the parameters.

For positron impact, the TCSs show more structures than molecules studied previously. Two stepwise increases in the TCS due to the positronium formation at 6.8 eV and direct ionization at 13.8 eV are clearly visible. The origins of other small structures are not known, but may well be due to admixture of the shape resonances discussed in Section III.E. Below about 3 eV down to 0.8 eV, the positron TCS becomes larger than the electron one, i.e., there is a reverse effect as in the case of NH_3. This effect in CO_2 has been examined in some detail by Kimura et al. [16,115] in conjunction with rovibrational excitation, which is discussed in Section IV.D below.

2. *Medium-Size Molecules*

a. Molecules With a Methane-Like shape. Of the CH_4, CH_3F, CH_2F_2, CHF_3, CF_4, SiH_4, and CCl_4 molecules studied, all have the same tetrahedral molecular structure. Among this group, CH_3F (1.858D), CH_2F_2 (1.978D),

and CHF_3 (1.651D) are strongly polar molecules, while CH_4, CF_4, SiH_4, and CCl_4 are nonpolar molecules. Because of the polar and nonpolar nature, these two groups are expected to show quite different characteristics in electron and positron scattering dynamics. Furthermore, the presence of F atom introduces some additional interesting characteristics. TCSs are shown in Figures 18–22 for CH_4[35], CH_2F_2, CF_4, CCl_4, and SiH_4, respectively. For CH_4, the data obtained by the Detroit group are also included.

First, a series of molecules from CH_4 to fluoromethane (F-substituted methane) and to CF_4 is examined. For TCSs by electron impact, the well-studied shape resonance peak at 8 eV can be observed for all the molecules from CH_4 to CF_4. An additional peak arising from the shape resonance around 25–40 eV begins to emerge as an H atom is replaced by an F atom starting from CH_2F_2. The structure becomes the most conspicuous in CF_4, implying that the origin of this peak is attributed to the F atom. For CH_3F, the F-atom effect is too weak to show up, and the general shape is nearly identical to that of CH_4. For the nonpolar molecules CH_4 and CF_4, the cross section decreases at the lower energies of the 8-eV resonance peak, followed by the RT minimum at ~ 0.6 eV for CH_4 and 0.8 eV for CF_4. For the polar

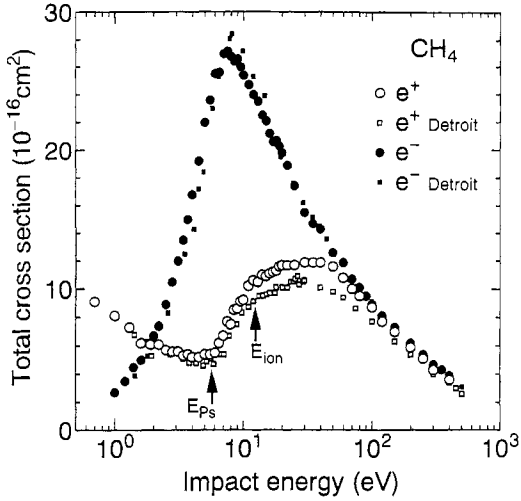

FIGURE 18. TCSs for electron and positron impact on CH_4. Solid circles, ●, are electron impact data by Sueoka and colleagues, and open circles, ○, are those of positron impact by Sueoka and colleagues. ■ are electron-impact TCS data by the Detroit group (Kauppila and Stein's group), and □ are those for positron impact by the Detroit group (Kauppila and Stein's group). Thesholds for Ps formation and ionization are indicated by arrows, respectively.

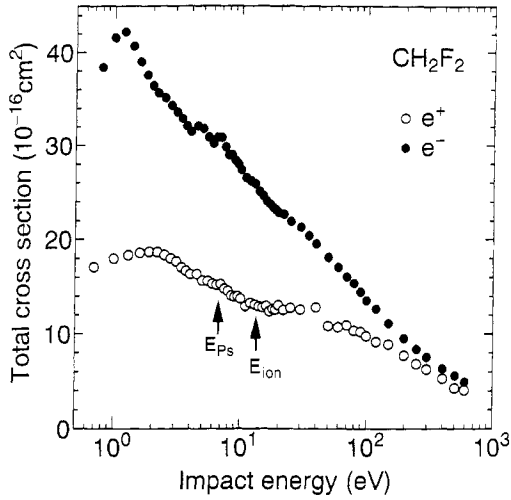

FIGURE 19. TCSs for electron and positron impact on CH_2F_2. Solid circles, ●, are electron impact data by Sueoka and colleagues, and open circles, ○, are those of positron impact by Sueoka and colleagues. Thesholds for Ps formation and ionization are indicated by arrows, respectively.

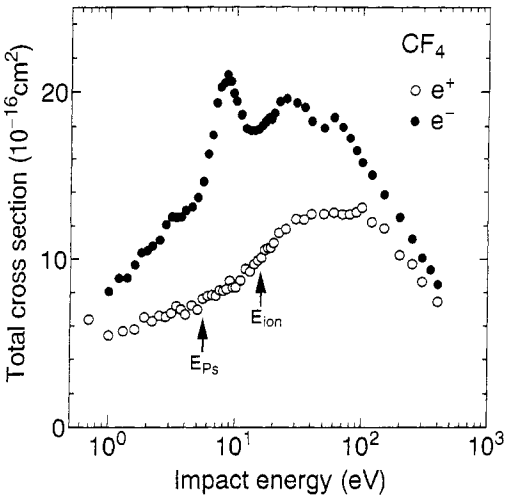

FIGURE 20. TCSs for electron and positron impact on CF_4. Solid circles, ●, are electron impact data by Sueoka and colleagues, and open circles, ○, are those of positron impact by Sueoka and colleagues. Thesholds for Ps formation and ionization are indicated by arrows, respectively.

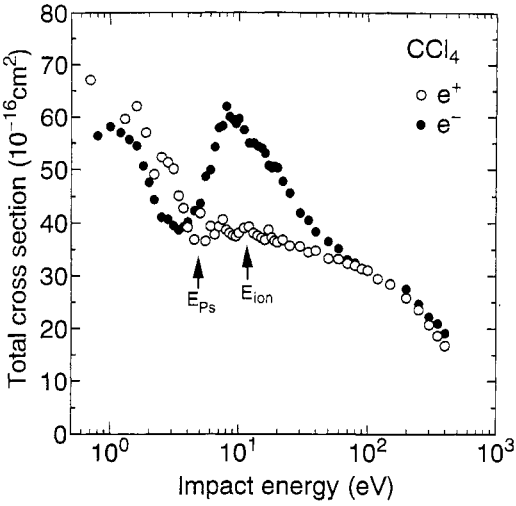

FIGURE 21. TCSs for electron and positron impact on CCl_4. Solid circles, ●, are electron impact data by Sueoka and colleagues, and open circles, ○, are those of positron impact by Sueoka and colleagues. Thesholds for Ps formation and ionization are indicated by arrows, respectively.

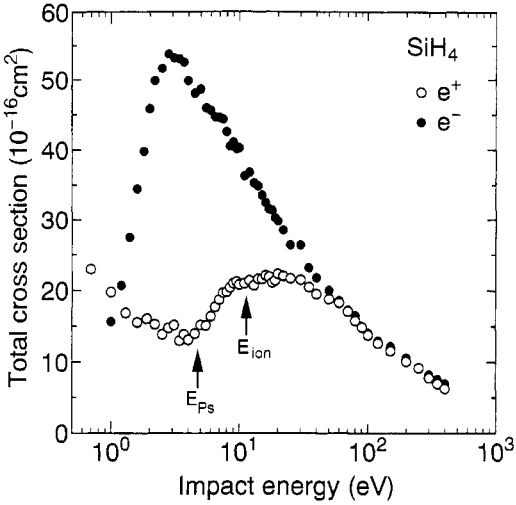

FIGURE 22. TCSs for electron and positron impact on SiH_4. Solid circles, ●, are electron impact data by Sueoka and colleagues, and open circles, ○, are those of positron impact by Sueoka and colleagues. Thesholds for Ps formation and ionization are indicated by arrows, respectively.

molecules, the TCSs continue to increase as the energy is lowered, a clear manifestation of the dipole effect. The same shape-resonance peak at 8 eV is known to be present in other fluoromethanes [116], but in addition, two broad peaks are observed clearly at around 20–30 eV and 50–60 eV. These peaks are due to the admixture of the contribution of an increasing number of partial waves and the availability of unoccupied molecular orbitals (UMOs) at higher energies [117].

It is worth commenting on the differential cross sections for the elastic electron scattering from the series of molecules from CH_4 to CF_4 obtained by Tanaka et al. [118], in order to better understand the electron scattering dynamics. A sharp rise at small angles below $50-60^\circ$ and a flattening at large angle beyond 140° in DCSs at 1.5 eV are observed for CH_3F, CH_2F_2, and CHF_3. This shows a distinct difference between polar and nonpolar molecules which is a direct consequence of the dipole moment. A hump seen around $70-80^\circ$ is due to the presence of the F atom, and the height of the hump increases as the number of F atoms increases to reach a maximum at CF_4, as exemplified by the 30-eV case. For the nonpolar cases of CH_4 and CF_4, the DCSs at 1.5 eV show a decreasing trend toward smaller angles after peaking at 60° due to the d-wave resonance. This is in contrast to the polar counterparts, although they again increase at much smaller angles. As the scattering energy increases above 100 eV or so, the differences are weakened rather drastically, and all DCSs are governed primarily by the molecular size or the size of the spatial electronic charge distribution.

For TCSs by positron impact, the maximum of the TCS generally shifts somewhat to the higher energy side of around 50–60 eV compared to that by electron impact (seen around 20–40 eV). This indicates that all inelastic processes are not necessarily effective in positron scattering until its scattering energy becomes high enough to be in the region where electron and positron TCSs begin to merge. The positron-TCSs for both CH_4 and CF_4 cross over their electron counterparts (at around 1.2 eV for CH_4 and 0.8 eV for CF_4), but this reverse phenomenon cannot be seen for other fluoromethanes within the present experimental energy limits. For the partial-fluoromethanes, two prominent peaks appear at around 2 eV and 40–50 eV. The magnitude of the TCSs becomes large with the replacement of more H atoms by F atoms. Below the first peak at 2 eV, the positron-TCSs decrease with decreasing energy. No sign of the turnover is seen, in contrast to these cases of CH_4 and CF_4, which eventually show the crossover to the electron-TCSs. For CHF_3, CH_2F_2, and CH_3F, the TCSs by electron and positron impacts appear to merge at a rather high energy above a few 100 eV. They stay parallel to each other below this energy down to ~ 150 eV [118]. It is interesting to note that the energy at which the electron- and positron-TCSs begin to merge becomes higher as the molecular size increases.

Additional cases of a similar trend seen clearly in larger hydrocarbons are presented later in this article.

TCSs for both electron and positron impacts for SiH_4 are very similar to those of CH_4, apparently because the Si atom and the C atom belong to the same atomic group in the periodic table, and hence the atomic structure of the valence electrons is similar. For the electron TCS, the only minor difference noticeable is the shift of the 8-eV shape resonance to a smaller energy of 3 eV for SiH_4. For the electron TCS, the shapes of the two cross sections are nearly identical to each other, although the magnitude is different. The merging of the TCSs for electron and positron for CH_4 and SiH_4 takes place at much lower energy (at the 60–70-eV region) than for other molecules considered in this group. Jain [119,120] has determined both the electron and positron TCSs theoretically. His results are in reasonable agreement with experiment in the energy region from 4 eV to 400 eV. Their elastic cross section indeed becomes energy-independent up to 40–50 eV, supporting the argument made above that inelastic channels are less effective at intermediate energies.

Lastly, we compared TCSs of CCl_4 with other molecules mentioned above, particularly with CF_4, in Figure 21 because the two have analogous electronic structures. For electron scattering, the TCS for CCl_4 has two large peaks due to the shape resonances at around 1 eV and 8 eV.

The marked and very interesting difference of the CCl_4 molecule from others can be seen in particular in positron-TCSs. For any TCS from CH_4 to CF_4, the positron-TCSs in general, have, a broad peak in the region of 30–100 eV, followed by a slow decrease at the lower energy side before they increase again at around a few eV. In contrast to this feature, the TCS for CCl_4 shows a slowly decreasing trend at energies higher than 5–6 eV, and it drops much faster below this region, i.e., it keeps decreasing at all the energies studied. There are a couple of structures at 7 eV and 12 eV due to positronium formation, electronic excitation, and direct ionization. The probable cause for the difference in this feature of the positron-TCS from those of other molecules is the large difference in the number of electrons, and hence the greater number of attractive wells available. In addition, the polarizability of CCl_4 ($11.2\times10^{-24}\,cm^3$) is larger by more than a factor of two than those of CF_4 ($3.838\times10^{-24}\,cm^3$), SiH_4 ($5.44\times10^{-24}\,cm^3$), and CH_4 ($2.593\times10^{-24}\,cm^3$). This may also contribute to the difference in the features of TCS.

The reverse of the TCSs for electrons and positrons in CCl_4 takes place at the rather higher energy of 4–5 eV compared to other molecules, most of which occur at around 1–2 eV. The reverse situation of the cross sections in CCl_4 still persists even at the lowest energy (0.7 eV) in the present measurement. As a result of its having been studied in radiation chemistry,

CCl_4 is known to be an effective electron scavenger in liquid, which might reduce the positronium formation rate in CCl_4; there is relevant discussion of this point in Section IV.F below. All these characteristics of CCl_4 are a reflection of the difference of the polarizability and electron-affinity from that of other molecules. This characteristic is significant for the further understanding of the physical and chemical phenomena of electron– and positron–liquid and solid phases in which this molecule is involved.

b. SF_6. SF_6 has been discussed in detail by Kauppila and Stein [14] the TCS, and so it is treated only briefly here. The TCS for electron impact shows several prominent peaks in the energy region from 1 – 50 eV, and the origin of these peaks has been identified by Lynch et al. [111] using the CMS calculation. These structures result from the combined contributions of different symmetries. Contrary to the electron TCS, the positron TCS is rather structureless, with the exception of a broad and weak peak at around the 20–30 eV region. This peak is due to the combination of Ps formation, electronic excitation, and direct ionization. Further, it appears that the positron TCS shows additional structures in the region of 3–10 eV. These structures may be due to the contribution of Ps formation from different orbital electrons. The two TCSs do not begin to merge at energies lower than 500 eV, and even at the highest energy studied, they appear still to be different.

c. Hydrocarbons: The Bonding Effect. The C_2H_2, C_2H_4, C_2H_6, and C_2F_6 molecules are nonpolar and have a triple-bond, double-bond, or single-bond, with light (H) or heavy (F) atoms attached to two central carbon atoms. Hence, some information on the effect of the bonding and charge distribution on TCSs as well as the fluorination effect can be extracted from a comparison of them. TCSs for C_2H_2, C_2H_4, and C_2H_6 are shown in Figures 23 – 25, respectively [35,121]. Bielefeld group has also studied some of these molecules [122].

First, the TCSs for C_2H_2, C_2H_4, and C_2H_6 may be compared for electron and positron impacts. For electron scattering, an existence of two strong shape-resonaces has been known, and the dominant peak seen at around 2 eV decreases in the order from C_2H_2 to C_2H_4 to C_2H_6, while the second peak at around 8 eV begins to grow in the order from C_2H_2 to C_2H_4 to C_2H_6. These two peaks become comparable in size at C_2H_4, and then the magnitude reverses at C_2H_2. These trends are a direct consequence of the capture of an electron into the $b2g$ (π^*), and $3a$ UMOs, or in other words, the difference of the electron charge distribution in the C–C bond; because of the higher density of electrons in the C–C triple-bond in C_2H_2, the incoming electron can attach loosely in the region close to the H atom through the

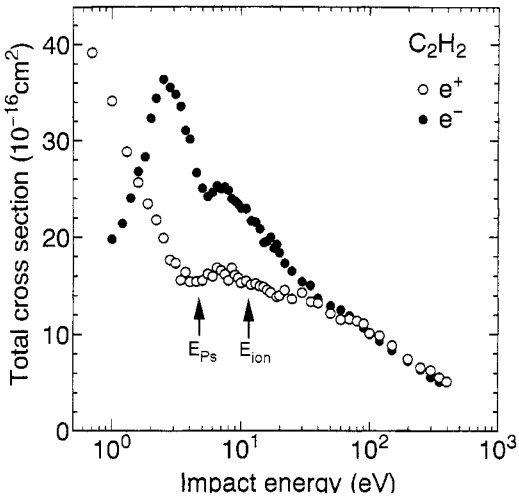

FIGURE 23. TCSs for electron and positron impact on C_2H_2. Solid circles, ●, are electron impact data by Sueoka and colleagues, and open circles, ○, are those of positron impact by Sueoka and colleagues. Thesholds for Ps formation and ionization are indicated by arrows, respectively.

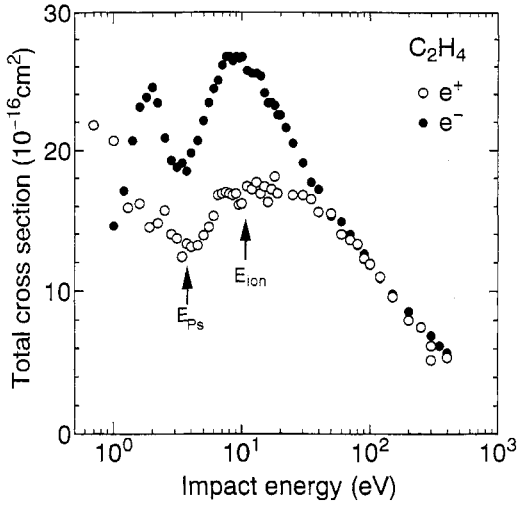

FIGURE 24. TCSs for electron and positron impact on C_2H_4. Solid circles, ●, are electron impact data by Sueoka and colleagues, and open circles, ○, are those of positron impact by Sueoka and colleagues [35]. (Note that the forward scattering correction is not included.) Thesholds for Ps formation and ionization are indicated by arrows, respectively.

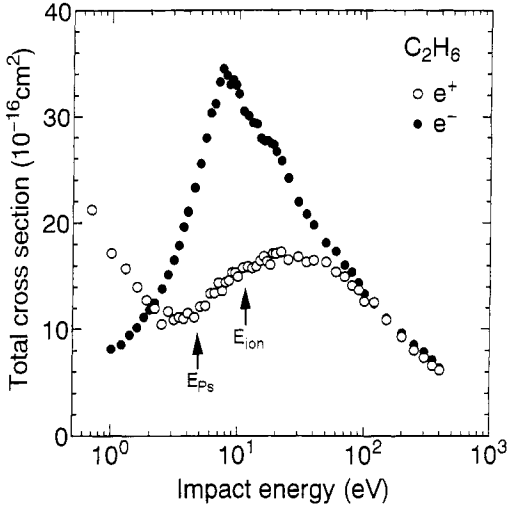

FIGURE 25. TCSs for electron and positron impact on C_2H_6. Solid circles, ●, are electron impact data by Sueoka and colleagues, and open circles, ○, are those of positron impact by Sueoka and colleagues [35]. Thesholds for Ps formation and ionization are indicated by arrows, respectively.

shallow potential well (shape resonance). As the electron concentration decreases from a triple- to double- to single-bond, the incoming electron can be trapped more often in the well near the C–C bond, resulting in the growth of the shape-resonance at 8 eV as the number of H atoms increases.

In Figure 26, the relation between the number of C atoms and the magnitude of the electron TCS is illustrated for CH_4, C_2H_2, C_2H_6, and C_3H_8. Except for a conspicuous peak at 2.5 eV for C_2H_2, the magnitude of the major peak at around 8 eV is in the order of $C_3H_8 > C_2H_6 > C_2H_4 > C_2H_2 > CH_4$, and at higher energy above 10 eV, this feature remains. This clearly demonstrates that as the number of C atoms increases, the TCS becomes generally larger, reflecting the molecular size. This feature is useful as a means of determining the molecular structure.

For positron impact, the positronium formation at around 7 eV, electronic excitation in the neighborhood of 8–9 eV and direct ionization at 12 eV are visible in C_2H_2, and to a lesser extent, in C_2H_4. But they are buried in the tail of a large broad peak and are not clearly seen in the case of C_2H_6. This phenomenon appears to be part of a general trend for larger molecules. In such molecules, an incoming positron may find that more shallow wells and more rovibrational states are available for extra energy dissipation. The result is that the positron tends to settle in temporarily rather than to form a positronium. This causes formation of weaker structures, on the whole. The

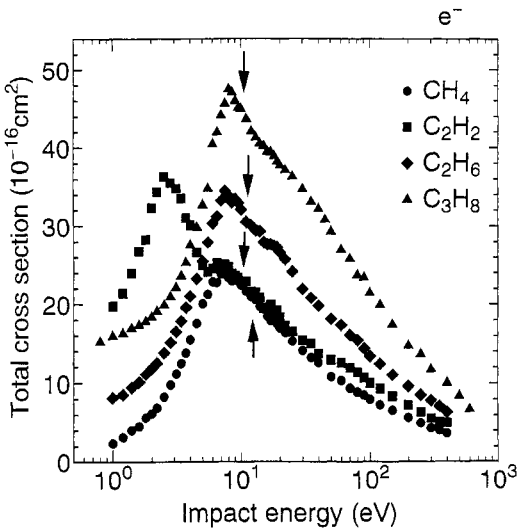

FIGURE 26. Electron-TCSs for CH_4, C_2H_2, C_2H_6, and C_3H_8 are displayed to illustrate the correlation between the strength of the TCS and the number of C atoms, or molecular size. The data are from Sueoka and colleagues [35,121]. Thesholds for Ps formation and ionization are indicated by arrows, respectively.

broad peak at around 20 eV apparently grows and shifts to higher energies in the order of $C_2H_6 > C_2H_4 > C_2H_2$. All three TCSs for positron scattering cross over those for electron impact in the region of at energies 1.5–2 eV.

Next, a comparison between C_2H_6 and C_2F_6 may be made. The electron TCSs for C_2H_6 and C_2F_6 are quite similar to those of CH_4 and CF_4, respectively, for electron scattering: a sharp resonance peak at 7–8 eV for the CH system, with two peaks at each 7–8 eV and 20–30 eV for the CF system. For positron impact, the TCSs for C_2H_6 and C_2F_6 are also similar to those for CH_4 and CF_4 in respect to general shape and features. These similarities between CH_4 and C_2H_6 and between CF_4 and C_2F_6 suggest that the influence of the C–C bond to the scattering is rather weak, but the same partial structure (i.e., CH_3 and CF_3) of CH_4 and C_2H_6 and the F-containing counterparts is the factor most responsible for the scattering effects. Apparently the molecular electron cloud on the C–C single bond is not dense enough to make a significant contribution to the dynamics compared to that in the double or triple C–C bond in molecules in this group.

3. Large Molecules

a. Butane and Propene, and Their F-Replaced Molecules. The molecules C_3H_8, C_3F_8, C_4H_8, and C_4F_8 are discussed here. First, the C_3H_8 and C_3F_8 systems are treated, followed by the C_4H_8 and C_4F_8 systems, with additional

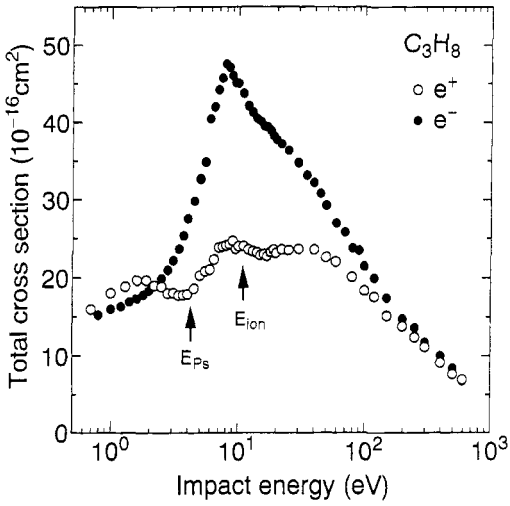

FIGURE 27. TCSs for electron and positron impact on C_3H_8. Solid circles, ●, are electron impact data by Sueoka and colleagues, and open circles, ○, are those of positron impact by Sueoka and colleagues [117]. Thesholds for Ps formation and ionization are indicated by arrows, respectively.

remarks on the comparison of C_3F_8 and C_4F_8. Figures 27 and 28 show TCSs for C_3H_8, and C_3F_8, respectively.

New aspects of electron scattering from C_3H_8 and C_3F_8 can be summarized as follows [117].

(1) Both C_3H_8 and C_3F_8 cross sections have a peak at around 8–9 eV. The cross section for C_3F_8 has a second peak near 25 eV. The first peak observed at 8–9 eV is common to other hydrocarbons and is due to a shape resonance arising from a temporary trapping of the electron in antibonding C–H orbitals. The second peak in C_3H_8 at 25 eV is due to a combination of shape resonances corresponding to a few of higher unoccupied orbitals in this energy region. It appears that C_3F_8 has a weak peak at around 3 eV.

(2) Both the cross sections decrease rather sharply as the energy decreases below 7–8 eV. Since these are polar molecules (with the value of the dipole moment being 0.084D and 0.097D for C_3H_8 and C_3F_8, respectively), their cross sections should increase again toward lower energies, based on the Born argument, as shown in Eq. (3.32).

(3) Both the cross sections also decrease gradually with increasing energies beyond the first (second) peak for C_3H_8 (C_3F_8) above 25–30 eV.

(4) Except for the region of 6–18 eV, the cross section for C_3F_8 is consistently larger than that for C_3H_8. At both ends of the energy range

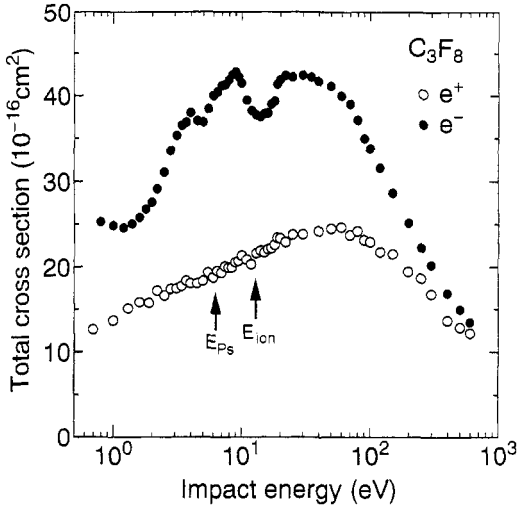

FIGURE 28. TCSs for electron and positron impact on C_3F_8. Solid circles, ●, are electron impact data by Sueoka and colleagues, and open circles, ○, are those of positron impact by Sueoka and colleagues [117]. Thesholds for Ps formation and ionization are indicated by arrows, respectively.

studied, the difference is nearly a doubling. This large difference in magnitude may be a reflection of the difference of the sizes of H and F atoms.

The results for positron scattering, are also included in Figures 27 and 28. Specific features for this case [117] are summarized here.

(1) The shapes of the cross sections are rather different below 50 eV. For C_3H_8, the cross section has three visible structures at around 3 eV, 8 eV, and 30 eV, while for C_3F_8 it is much smoother except for a maximum at around 40 eV. It is interesting to note that the peak position of 8 eV in C_3H_8 for positron impact is nearly the same as that for electron impact. The peak for electron impact is due to a shape resonance, while that for positron impact is formed by the combination of Ps formation and electronic excitation. Nevertheless, this coincidence of the peak positions may warrant further investigation.

(2) The maximum magnitude of the cross sections is rather similar. Both appear to measure approximately $2.2\times10^{-15}cm^2$ at the peak at around 20–30 eV. The cross section for C_3H_8 drops somewhat faster at higher energies than that for C_3F_8, and at 500 eV, for example, the cross section for C_3H_8 reaches $8\times10^{-16}cm^2$ while that for C_3F_8 is approximately 12×10^{-16} cm^2. This difference in the behavior at higher energies is a consequence of the

size of the molecule, as well as the stronger interaction of the F atoms for the incident positron.

The definite cause of the three strong peaks seen in C_3H_8 is not yet obvious. However, for the peak at 3 eV, we suspect that a positronic pentane ($Ps–C_3H_8$) may possibly be formed by temporarily trapping the positron in the outer tail of the molecular field, or by the Feshbach-type resonance. For C_3F_8, the F atom has a stronger electron negativity than a carbon atom, so that the F atom charges negatively, in contrast to positively charged H atoms in C_3H_8. Therefore, an incoming positron senses more negative charge when it approaches C_3F_8. These electrons could wrap up the incoming positron to form a temporal resonance state. This resonance state is not stable, and it decays through the effect of two γ-ray emissions. Based on a simple general formula for the annihilation rate [123], the approximate rate can be estimated to possess a value of the order of 10^{10}sec^{-1}, which is about four times faster than that of the PsH complex owing to the presence of a larger number of electrons in the former molecule.

Some unique features emerge when a comparison is made between these two sets of the results, summarized as follows.

(1) The magnitude of the total cross sections for C_3H_8 for positron impact is far smaller than that for electron impact in the region of intermediate energy, which amounts to less than a half. The situation reverses below a couple of eV for C_3H_8. That is, the positron TCS is larger than the electron TCS. This feature may be due to a larger cross section for some channels in rotational excitations by positron impact than that caused by electron impact, as the authors have pointed out earlier [16].

(2) In contrast, the magnitude of the total cross section of C_3F_8 for positron impact is consistently smaller than that of electron impact at all energies studied, and no reverse of this situation is found in the magnitude of the cross section. We speculate that for C_3F_8, the rovibrational energy spacing is smaller than that for C_3H_8. Hence, the reverse of the cross section may take place at much lower energy (much closer to the threshold). The experimental confirmation of this explanation is difficult to achieve, since the energy range in which the reverse phenomenon can be seen is too low, given present experimental limitations.

(3) Both the positron and electron impact cross sections appear to merge beyond 200 eV, which is slightly higher than would be the case for small molecules. However, the behavior of the two sets of the cross section for electron and positron impacts is vastly different for different molecules. The difference for C_3H_8 becomes much smaller at lower collision energy of 30–40 eV, while it begins to narrow only beyond 100 eV for C_3F_8. This disparity

is apparently a reflection of the size of the charge distribution of H and F atoms. In other words, we can in effect "see" the wave functions of C_3H_8 and C_3F_8 by comparing electron and positron impacts.

Lastly, in reference to the comparison between the C_3F_8 and C_4F_8 molecules, the electron-TCSs for each of the two molecules are similar in general shape, i.e., one large and broad peak in the energy region of 4–100 eV, and a couple of small structures at around 8–9 eV and 20–30 eV. At lower energies of the peak, it has a minimum, but goes back up again at much lower energies. The structure on the large hump is more visible for C_3F_8, whereas the magnitude of the broad peak is slightly larger (by less than a few percentage points) for C_4F_8. This difference in magnitude and structure may represent the effect of an additional C atom. For the positron-TCS, again, both structure and function look similar for each of the two molecules in general, but they differ slightly in their details. For C_4F_8, the small structure around 6 eV is more conspicuous and stronger than that in C_3F_8. Normally the structure becomes weaker for a larger molecule. However, C_4F_8 does not follow this general rule. This would mean that the origin of the clearly visible structure may relate to the degree of the spatial spread of its molecular configuration or to the steric effect of the molecule. This anomaly may be another interesting point on which a further study should be solicited. Lastly, for both the molecules, no reversed phenomenon of TCSs for electron and positron impacts is seen at any energy region presently studied.

b. Alcohol. The CH_3OH, and C_2H_5OH alcohol molecules have an intermediate dipole moment. The TCSs for these two molecules are very similar, and hence a general set of features for these molecules can be summarized here. TCSs for the CH_3OH are displayed in Figure 29.

For electron scattering, two rather conspicuous peaks are observed at around 2 eV and 8 eV, respectively, which are attributable to the shape resonance commonly seen in most of carbon-containing molecules already discussed. The TCSs below 1.5–2 eV show an increasing trend, clearly reflecting the dipole moment effect, as explained above in connection with Eq. (3.32). The height of the second-peak at 8 eV is larger for C_2H_5OH than that of CH_3OH by 25%, due primarily to the effect of an additional C atom. The overall magnitude of the TCS for C_2H_5OH is larger in the entire energy region, reflecting the molecular size.

For positron impact, the cross sections are always smaller than those for electron impact and have many small structures in the region of 5–15 eV which are due to the combination of the positronium formation (perhaps from different valence shells), electronic excitation, and impact ionization. The origin of a rather strong peak at around 1.2–1.5 eV for both the

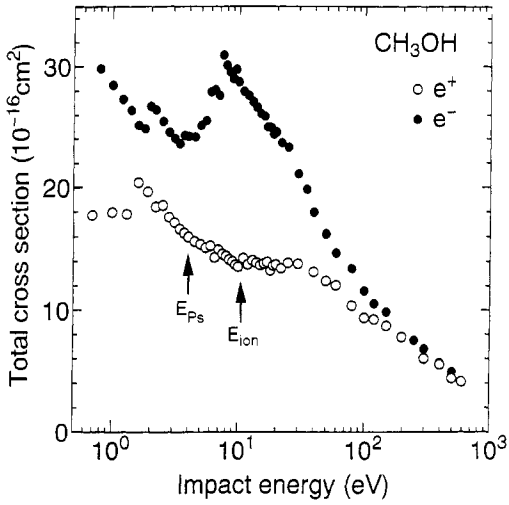

FIGURE 29. TCSs for electron and positron impact on CH_3OH. Solid circles, ●, are electron impact data by Sueoka and colleagues, and open circles, ○, are those of positron impact by Sueoka and colleagues. Thesholds for Ps formation and ionization are indicated by arrows, respectively.

molecules is not clearly known, but as speculated earlier for other molecules, it may well be a resonance due to a temporary capture of the positron within a molecule. Apart from these structures, the TCSs are relatively smooth. Positron-TCSs and electron-TCSs appear to merge reasonably well above 200 eV for these molecules. At lower energies, there seems no clear sign of the occurrence of the reverse effect of the cross sections. Based on the Born argument for a polar molecule, the TCSs should increase eventually at sufficiently low energies.

c. Formic Acid and Acetic Acid. The formic acid and acetic acid molecules HCOOH and CH_3COOH, have an intermediate dipole moment with a common COOH-group. TCSs are shown in Figure 30 for HCOOH.

The TCSs for the two molecules for electron impact are quite similar in some respects, but there are a few differences. Both cross sections have two major peaks, which are due to shape-resonances. For HCOOH, the cross section has a very small peak at 1.8 eV and a broader one at around 7–15 eV. For CH_3COOH, the TCS has two rather sharp peaks at 2 eV and 8 eV, respectively, both of which share the characteristics common to most of the carbon-containing molecules. Even though the dipole moment of HCOOH is weaker than that of CH_3COOH, the TCS for HCOOH already shows the characteristic of polar molecules below a few eV, while that for CH_3COOH appears to be rather flat below the first resonance peak at 2 eV. The

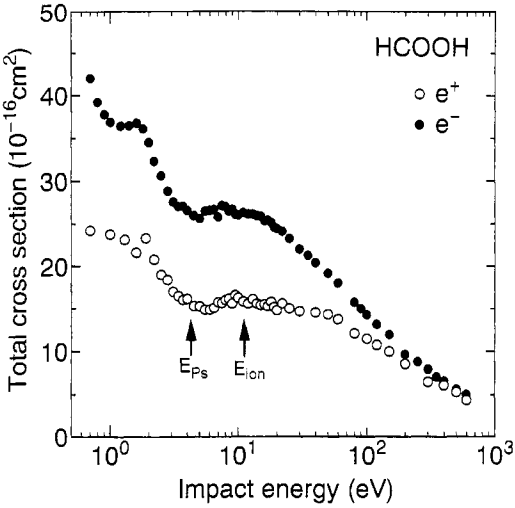

FIGURE 30. TCSs for electron and positron impact on HCOOH. Solid circles, ●, are electron impact data by Sueoka and colleagues, and open circles, ○, are those of positron impact by Sueoka and colleagues. (Note that the forward scattering correction is not included.) Thesholds for Ps formation and ionization are indicated by arrows, respectively.

magnitude of the TCS is larger for CH_3COOH than for HCOOH above 100 eV or so, reflecting the different molecular size. Except for the sharp peak at 8 eV for CH_3COOH, however, the magnitude of the cross section generally becomes larger for HCOOH, particularly below 2–3 eV.

For positron-TCSs, the similarity and difference can again be seen. In the TCS, many small structures due to positronium formation (from different valence shells), electronic excitation, and direct ionization are common in the range of 5 to 20 eV. A rather strong peak at 1–2 eV can also be seen for CH_3COOH, while for HCOOH, the corresponding peak is much smaller, but somewhat sharper. However, the peak at 1.8 eV for HCOOH is considered to be superposed on a much broader hump below 2 eV. The peaks at the low energy side are probably due to the positron-resonance, as described above. For HCOOH, the positron-TCS also shows the effect of dipole moment below 1 eV, while that for CH_3COOH has not reached the region yet. Generally, the magnitude of the positron cross section of CH_3COOH is larger than that of HCOOH, and more abundant structures are apparent in the former.

d. Acetone. The acetone, $(CH_3)_2CO$, molecule belongs to the ketone group, having the molecular structure of CH_3–CO–CH_3, and it has a rather strong dipole moment. TCSs are shown in Figure 31.

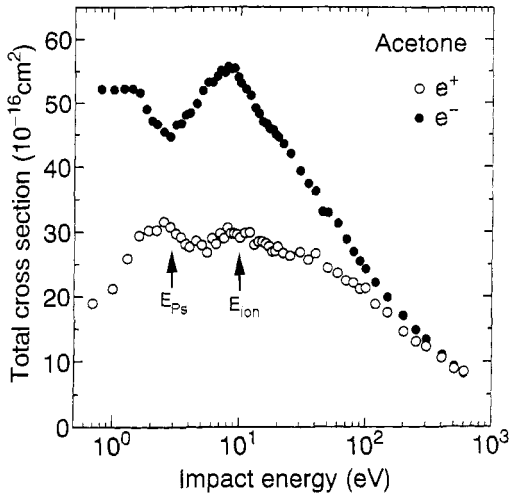

FIGURE 31. TCSs for electron and positron impact on aceton. Solid circles, ●, are electron impact data by Sueoka and colleagues, and open circles, ○, are those of positron impact by Sueoka and colleagues. Thesholds for Ps formation and ionization are indicated by arrows, respectively.

For acetone, the electron-TCS has two marked peaks, at around 1.5 eV and 8 eV, respectively. The second peak is common to all hydrocarbons and their relatives, and is due to the shape resonance repeatedly discussed above. The first peak at lower energy appears to level off and to flatten at the lower energy side. However, because of its polar nature, it should go up at much lower energies.

The positron-TCS is consistently smaller than that for the electron. It levels off in magnitude at intermediate energies and even undergoes a decreasing magnitude, with decreasing energy below 2 eV. The peak near 1.8 eV, commonly seen in all other large molecules, is also observed. The feature of a very small positron TCS may come from the additional O atom for acetone. The strong electron affinity of the O atom reduces the electron charge distribution around the H atom, leaving it more positively charged ion. Hence this effectively reduces the scattering event for incoming positron, resulting in the small TCS. For the positron-TCSs, the structure due to positronium formation, electronic excitation, and direct ionization is rather marked. The structure at low energy is shifted to a somewhat higher energy of 3 eV, and for much lower energies (below 1.5 eV), the TCS decreases rather drastically, features that are absent for other large molecules. It should noted that the energy at which electron- and positron-TCSs merge is much higher for acetone. In fact, the merging occurs beyond 300 – 400 eV, which may be due to the weaker interaction.

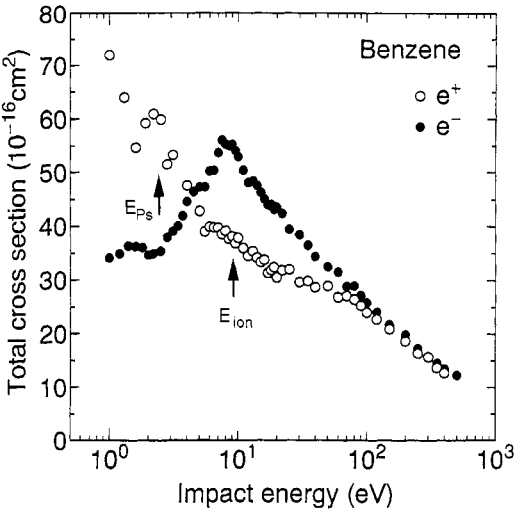

FIGURE 32. TCSs for electron and positron impact on C_6H_6. Solid circles, ●, are electron impact data by Sueoka and colleagues, and open circles, ○, are those of positron impact by Sueoka and colleagues. Thesholds for Ps formation and ionization are indicated by arrows, respectively.

e. Benzene and Toluene. Toluene, $C_6H_5CH_3$, is a polar molecule, while benzene, C_6H_6, is a non polar molecule [124]. The TCSs for C_6H_6 are displayed in Figure 32.

Benzene and toluene show a very close similarity, typified by the electron and positron impact on C_6H_6 shown in Figure 32, i.e., each has a very strong peak at 9–10 eV with an additional small structure around 1.5–2 eV. The two molecules show a strong resemblance for positron scattering as well. The positron-TCSs increase rather monotonically as the energy is lowered, and display few structures in the energy region of 5–20 eV. They cross over the electron-TCSs at the neighborhood of 4 eV and become far larger than electron-TCSs below 4 eV. The difference between the electron- and positron-TCSs may be the largest among the molecules studied so far. The magnitude of the difference is nearly a factor of 2 for benzene and 1.5 for toluene at 1 eV, for example. The electron-TCSs show no sign of increase with decreasing energy below 2–3 eV. This observation may be due to the increasing number of rovibrational states that become available as the molecular size increases. For positron scattering, some of these excitation channels may be more efficient and far outnumber the electron-scattering counterparts. The positron-TCS for toluene shows a peak at 1.5 eV, followed by the drop at lower energy side, while for benzene, it also shows a rather sharp peak near 1.8 eV, but also a sharp increase below 1.3 eV to much lower

energies. These peaks seen at around 1.5 – 1.8 eV are similar to those found in all other large molecular cases, indicating the possibility of a resonance. The electron and positron TCSs for molecules approach a level reasonably well above 100 eV for these systems.

f. Isomer Effect

I. PENTANE. Pentane, C_5H_{12} (normal-, iso-, cyclo-pentane) is also examined here because clear observation of an isomer effect is of particular significance. An examination of the isomer effect in the dynamics of electron and positron scattering is important for applications such as the determination of complex molecular structures. Figure 33 shows the representative result for TCSs for n-C_5H_{12}.

For electron scattering, the general features in TCSs for the three isomers are found to be very close to each other. The TCS has a major peak at 8 eV and a small shoulder at 25 eV. With decreasing energy, it decreases sharply but rather smoothly and levels off near the end of the present measurement at 1.5 eV. The height of the major peak at 8 eV is comparable for n- and iso-pentanes, but it is smaller by about 15% for cyclo-pentane. A second shoulder appears for cyclo-pentane and stands out more markedly for that of the other two molecules.

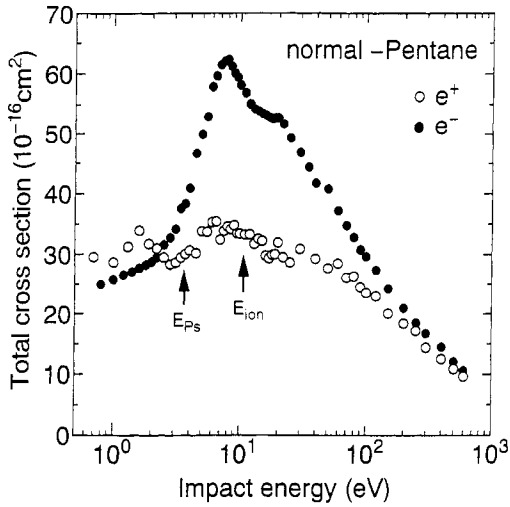

FIGURE 33. TCSs for electron and positron impact on normal-pentane. Solid circles, ●, are electron impact data by Sueoka and colleagues, and open circles, ○, are those of positron impact by Sueoka and colleagues. (Note that the forward scattering correction is not included.) Thesholds for Ps formation and ionization are indicated by arrows, respectively.

For positron scattering, small structures arising from positronium formation, electronic excitation, and ionization are also present for all the three isomers in the region of 6–20 eV. Except for these structures, the positron-TCSs are rather smooth as the collision energy is increased. In lower energy regions, a rather large peak is observed at 1.5–1.8 eV, which is a common feature for larger molecules as has repeatedly been mentioned. The peak may be due to the positron-in-molecule or resonance process, although this peak is somewhat weak for the cyclo-pentane. A reverse of the cross sections between electron and positron impacts occurs below 2.5 eV, and the difference is sizable for *n*- and iso-pentane. For the cyclo-pentane, the difference is not as large as for the other two molecules because of the smaller peak at 1.5 eV. In fact, the electron-TCS trend for the molecule turns to go up again and becomes dominant below 1 eV. For these collision systems, the isomer effect is found to be not so large, but certainly not negligible either. The reason for this weak isomer effect may be that the molecules considered are sufficiently large that there are many electrons and bonds that smear out the effect.

II. HEXANE. Hexane, C_6H_{12} (normal- and cyclo-), molecules have a benzene-ring structure with no double bond. TCSs for both the projectiles for normal- and cyclo-hexane are illustrated in Figures 34 and 35, respectively.

For *n*-hexane, the general feature of the electron-TCS is somewhat similar to the case of CH_4 and other large hydrocarbons, in which there is a large, pronounced peak at 8 eV and small, broad structures at around 15–25 eV. The peak that appears at 8 eV is the shape-resonance arising from an unoccupied π orbital, while the smaller structures at 20 eV are due to a combination of shape-resonances of higher symmetries. At the lower side of the peak, the TCS decreases rather smoothly with decreasing energy. It is flattened below 1–2 eV. For *c*-hexane, the peak at around 20 eV in the TCSs for electron impact becomes sharper and more pronounced compared to the TCS for *n*-hexane although the magnitude of the TCS for the former is in general smaller, reflecting the molecular structure and corresponding orbital energies.

For positron scattering, the *n*- and *c*-hexane TCSs have a few structures in the energy region between 6–20 eV, for the reason described above i.e., Ps formation, electronic excitation and ionization. The structures in *c*-hexane appear to be somewhat weaker. The peak at $\sim$8 eV energes more clearly for *n*-hexane, while that for c-hexane is weak but much broader (from $\sim$6 to 12 eV). A series of small structures beyond 12 eV appears in both the TCSs, due to a series of ionization channels. The TCSs for *n*-hexane and *c*-hexane show a conspicuous peak at around 1.5 eV, which is seen commonly in other

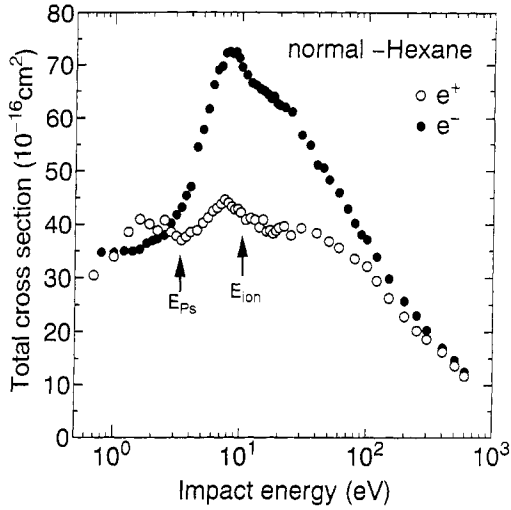

FIGURE 34. TCSs for electron and positron impact on normal-hexane. Solid circles, ●, are electron impact data by Sueoka and colleagues, and open circles, ○, are those of positron impact by Sueoka and colleagues. (Note that the forward scattering correction is not included.) Thesholds for Ps formation and ionization are indicated by arrows, respectively.

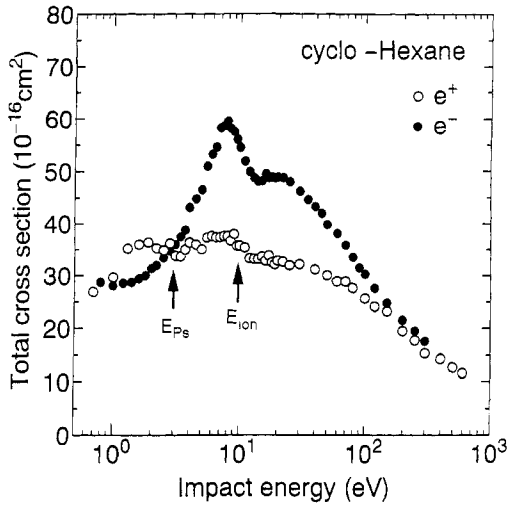

FIGURE 35. TCSs for electron and positron impact on cyclo-hexane. Solid circles, ●, are electron impact data by Sueoka and colleagues, and open circles, ○, are those of positron impact by Sueoka and colleagues. (Note that the forward scattering correction is not included.) Thesholds for Ps formation and ionization are indicated by arrows, respectively.

molecules, and then decrease with decreasing energy rather quickly below 1.0 eV. Hence, the reverse of the cross sections between electron- and positron-TCSs is found to take place for both the molecules only in a very narrow region between 3 eV and 1 eV. The merging of two TCS's for both the molecules occurs at rather high energy above 400 eV, posing an another interesting question, namely why the merging energy varies from system to system so drastically.

III. OCTANE. Octane, C_8H_{18}(normal-) and C_8H_{16}(cyclo-), are two isomers that have different molecular structures: the linear structure for normal-octane, and a ring shape for cyclo-octane, according to the presence of a differing number of H atoms. Similarly to other hydrocarbons, the electron-TCS for both the molecules has two peaks, a sharp peak at around 8 eV, and a broader but weaker peak at around 20–30 eV. At the lower energy side of the first peak, the TCS drops sharply. At the higher energy side above 50 eV, it decreases more gradually. The height of the first peak is 20% larger for normal-octane than that for cyclo-octane. The magnitude of the TCS remains large for normal-octane even at 600 eV, a clear reflection of the molecular size. The origin of the peaks is the shape-resonance repeatedly discussed above. For positron-TCSs, both the molecules show a peak at around 7–8 eV. This is due to the combination of positronium formation, electronic excitation, and ionization channels. The normal-octane and cyclo-octane molecules also have a weaker peak at around 30 eV. In the low-energy region of around 2–3 eV, a small structure emerges for both the isomers, and this might be due to the resonance, as described earlier. A marked difference between the two isomers is seen in regard to this small structure. That is, a sharper structure appears for cyclo-octane and a weaker one for normal-one. This difference clearly exemplifies the degree of molecular structure dependence. The magnitude of the positron-TCS for normal-octane is about 20% larger than that for cyclo-octane. This difference is similar to that seen in electron-TCSs. The general shapes in positron-TCSs for each of the two isomers are similar, but when examined in greater detail, it is apparent that there are many different features which are a manifestation of the isomer effect. A further systematic study from both the theoretical and experimental points of view is thus warranted.

B. Differential Cross Sections

It is obvious that differential cross sections (DCSs) will provide more detailed information of underlying scattering dynamics, and measurements for DCSs certainly serve as a more sensitive test of scattering theory than those of TCS. However, up to now, only three groups (Detroit, Bielefeld, and UCL) have successfully reported DCS measurements for positron scattering.

They have performed the measurement of the elastic process for atoms or simple molecules (i.e., H_2, CO_2, O_2, and CH_4) and positronium formation for atoms. In an intriguing result of the DCS study, Dou et al. [12] have extracted a resonance-like structure at scattering angles 60°, 90°, and 120° in the energy range of 55–60 eV in the elastic DCS for rare-gas and alkali atoms. They attributed the origin of the structure to a coupled-channel shape resonance, a type of resonance which appears if the coupling between elastic and Ps formation channels is considered.

Recently, Przybyla et al. [66,125] have performed DCS measurements for methane and CO_2 and compared electron- and positron-DCSs. Their results clearly illustrate that the Ps formation has a significant effect on the elastic scattering channel, as was shown earlier in Figure 10. They observed a minimum at around 60° and at 4 eV in elastic scattering. This minimum is mainly present in elastic scattering where the positron energy is below the Ps formation threshold and when the energy increases above the threshold, the minimum disappears faster than theory which considers only elastic scattering would predict. They point out the similarity of the DCSs of Ar and CH_4 for positron scattering, though a marked difference appears between electron and positron impacts. For electron impact, more structures are seen even at a high energy of 100 eV, while for positron impact, the DCS is rather structureless except at energies below the threshold of Ps formation. The presence of structures for electron and the absence of structure for positron are attributable to the combination of diffraction effects and the effect of the net attractive interaction.

Kövér and Laricchia [126] have reported the first measurement of triply differential cross sections of positron impact ionization of H_2. A small peak in the spectrum of the ejected electron was observed, which was interpreted as an evidence of electron capture to a continuum state of positronium.

Some theoretical studies of the DCS for positron scattering [127,128] have been reported. Although the results of the calculation they obtained by using a close-coupling method or R-matrix method are reasonably successful in reproducing the experiment and seem to provide some insight into the dynamics, a more rigorous and systematic study is undoubtedly required for further, improved understanding.

For positronium formation from atomic targets, Raith and his group at Bielefeld [129–131] have achieved a measurement of the angular dependence in positron–Ar and –Kr collisions from 0° to 120° in the energy region from 75 to 120 eV. They claimed to succeed in separating the positronium formation and positronium formation–ionization processes. An equivalent process is possible in ion–atom collisions, and indeed these latter have been studied extensively in order to examine the correlation effect. This dynamical correlation itself is an interesting subject in basic physics.

Unfortunately, however, no further experiment for this topic has been reported to date for molecular targets.

Although there are no reports on the DCS study for molecules larger than N_2, CO, O_2, N_2O, CO_2 [125], and the like, it would certainly be natural to believe that such DCSs as have been reported contain much important and interesting information indicative of new physics. This ongoing study will surely lead to and open up an exciting new field in atomic and condensed matter physics. In this sense, the further extension of the DCS investigation to larger molecules has a potential for finding new phenomena such as resonance, quantum effect, correlation effect, and a lot more that has not yet been discovered.

C. Ionization and Electronic Excitation

1. Ionization

A comparison of the electron-impact and positron-impact ionization of atomic targets has been made several times. Knudsen and Reading [132], for example, have discussed the comparison, particularly in terms of the difference in the threshold behavior. They included the experimental data for H_2 [56,133] in their comparison. The behavior of the ionization cross section of H_2 differs slightly from that of rare-gas atoms. Other than these atomic targets, as far as is known, there is almost no systematic experimental and theoretical study of ionization. As described briefly in Section II for impact ionization, the threshold behavior of electron and positron scattering is known to obey the Wannier law, and the cross-section form is given as,

$$\sigma_{\text{ion}} \sim (E - E_{\text{ion}})^n \tag{4.1}$$

The value of the exponent n for electron scattering has been the subject of vigorous experimental as well as theoretical study over the years, and is now reasonably well established to be 1.127. For positron scattering, the exponent values have been experimentally determined as 1.99 ± 0.19 for He and 1.70 ± 0.11 for H_2 which are larger than that of electron impact, but smaller than that of theoretical result (2.651) for positron impact by Klar [51]. Therefore, near the threshold, this formula suggests that electron impact ionization is less effective than that of positron impact. However, the measurement for ionization from rare gases and H_2 molecule by Raith and his colleagues [48,56] has appeared to show that the ionization cross section for positron impact is 10–15% larger than that for electron impact at intermediate energies from around 30 eV up to a few 100 eV. For higher energies above a few 100 eV, where these electron and positron ionization cross sections begin to merge, the ionization experiment has been of great

theoretical interest because the determination of the exact energy for the merging poses a challenge to theorists in terms of the validity of the first Born approximation. Furthermore, it also raises a question: If the merging energy varies from one target to another, then what causes this difference? As we have shown earlier, for some molecules, the merging energy of the two total cross sections is rather high (i.e., above 500–600 eV), while for others, these energies already begin to overlap even at levels as low as 100 eV. Clear understanding of this phenomenon requires further theoretical study as well as the experimental measurement of partial contributions to the TCS.

2. *Electronic Excitation*

The only known example of the calculation of the positron-impact excitation of the electronic state of a molecule is the excitation of B state of H_2. Mukherjee et al., [134] applied a two-state close-coupling method to the calculation of the excitation cross section. Then, in 1994, Lino et al. [20] used the Schwinger multichannel method to obtain the differential, as well as integral, cross sections for the excitation of the B state. There is a large disagreement between the integral cross sections obtained by the two groups. The difference may be ascribed to the description of the excited state in the two calculations. It should be noted that the DCSs obtained by Lino et al. at 20 and 30 eV are similar to those for the excitation by electron collisions. The authors ascribed this similarity to the fact that the excitation of the B state is governed mainly by a dipole transition.

The interesting difference in the positron and the electron impact excitations of the electronic state is that only singlet states can be excited by positron, if the molecule is initially in its singlet state. This produces a significant distinction between the energy loss spectra in the positron– and the electron–molecule collisions. Furthermore, in many closed-shell molecules, triplet states are repulsive and an excitation of those states (through electron exchange) eventually leads to dissociation of the molecule. For example, excitation of the lowest triplet state, $b\ ^3\Sigma$, of H_2 plays a principal role in the dissociation process of the molecule [135]. In this sense, positron impact is less effective in the dissociation of molecules than an electron collision, because of the absence of electron exchange.

It is interesting to note, and may perhaps be significant that available experimental evidence for atomic cases suggests that electronic excitation is also larger for positron than for electrons, at least above the intermediate energy region. It appears that the attractive Coulomb interaction between incoming positron and target electrons might enhance electronic excitation over whatever countervailing effect the repulsive incoming electron–target electron interaction has. Certainly, more careful analysis and an extensive

study of electron–electron and positron–electron correlations should be carried out before any definitive conclusion is drawn.

D. Vibrational and Rotational Excitation

Vibrational excitation of molecules by electron impact often proceeds via an intermediate negative ionic state (resonance). Vibrational excitation through the resonance causes a variety of structures and a large cross section. For positron impact, any existence of such a resonance state is not supported by direct experimental measurement. Therefore, vibrational excitation cross sections for positron impact are normally estimated to be small and rather smooth. Furthermore, there are few systematic and comparative studies based on theoretical calculations, except those made for some small molecules. Recently Kimura et al. [16] carried out a joint theoretical and experimental study for vibrational excitation of CO_2 for electron and positron impacts at 2 eV, 5 eV, and 6 eV. For the (100) symmetric stretching excitation, it was found that the cross section by electron impact is larger by almost three orders of magnitude than that by positron impact, while the cross sections for (010) bending and (001) asymmetric stretching excitations are nearly identical for electron and positron impacts. This theoretical finding is substantiated by the experiment using an energy-loss technique, where the sum of the cross sections for all three vibrational modes for electron impact is found to be larger by a factor of five than that for positron impact. This surprising result is supported by a rationale based on the wave function of the incident projectile and coupling matrix element; if the coupling is strong and of long range like the dipole interaction, then it is not so crucial that the projectile penetrate deeply into the molecule in order to interact effectively. But if the coupling is weak and short-range in nature like the polarization interaction, the interaction is more sensitive to how far the projectile can penetrate within a molecule in order to have an efficient interaction. For positron, the repulsive static interaction prevents it from approaching closer to nuclei, resulting in a smaller disturbance to the nuclear motion and hence weaker interaction. As a result, less vibrational transition takes place. For the (100)-excitation, similar characteristics of the cross section have been reported by Gianturco and colleagues [114]. More recently, Surko's group measured vibrational excitation for CF_4 [136] and their result was found to be consistent to that of CO_2 [16].

Jain [137] has studied a vibrational excitation of CO molecule by positron impacts below the Ps formation threshold. He adopted a close-coupling method and the first Born approximation to examine the excitation to $v' = 1$ and 2 levels. His results of the two methods are generally in qualitative accord with each other over the entire energy region studied. This is because the positron–CO interaction is weak. Comparing his results with those of

electron scattering obtained by Morgan [138] based on the R-matrix method, he found that vibrational excitation to $v' = 1$ level by electron scattering is larger by an order of magnitude than that of positron scattering at above 3 eV. Near about 2 eV where the CO molecule possesses a strong peak due to the shape resonance, the difference widens by nearly two orders of magnitude, because the cross section for positron impact does not induce any resonance in this energy domain. The rationale for this observation should be similar to that discussed above in the case of CO_2.

There have been a few calculations on rotational excitations of molecules by positron impact made by using either the perturbative method or close-coupling method. Earlier, Takayanagi and Inokuti [1] investigated the rotational excitation by electron and positron impact by using the Born approximation, and found that for diatomic molecules with a negative quadrupole moment, the rotational excitation cross section caused by positron impact should be larger than that caused by electron impact as exemplified above in Eq. (3.29). They showed some representative results for cases such as H_2 and N_2. Jain and Thompson [110] have shown some results for rotational excitation of CH_4 molecules for electron and positron impacts, based on a close-coupling approach with a model potential. In this work, for rotational excitation they have found that for $J = 0 \rightarrow 3$ that positron scattering constantly gives a larger cross section than that of electron impact at just above threshold to 7 eV. For the excitation of $J = 0 \rightarrow 4$ transition, on the other hand, the situation is reversed, and the electron scattering is found to have a larger cross section. The reason for this reverse effect is not clearly stated in the published study. However, since these cross sections are very sensitive to the interaction potential employed, the possibility that this effect may be an artefact cannot be entirely ruled out. There are some other calculations for rotational excitation processes of various smaller molecules such as CO made by using the close-coupling or R-matrix methods, but those results were considered to be test studies of interactions and other parameters and may be regarded as preliminary.

E. Positronium Formation and Positron Attachment

As a general rule, the peak in total cross section due to Ps formation tends to weaken, or to become less apparent, as the size of the molecule (or the number of electron) increases, although there are, of course, some exceptions. This tendency may be understood by the process of positron attachment in which a large number of electrons wrap up the positron to form a quasi-bound state within the molecule, or a few shallow potential wells trap the positron. The excess energy arising from the sum of the positron kinetic energy and the molecular affinity is efficiently absorbed and distributed among many rovibrational levels, which are more readily

available in larger molecules. As the molecular size increases, this condition is more likely to be realized. For smaller molecules, the phenomenon is less likely to take place, because the number of electrons available for wrapping up positron is limited and the excess energy is not easily dissipated within the molecule. Hence, the direct positronium is preferably formed. Indirect evidence of this phenomenon was first pointed out by Paul and Saint-Pierre [102] through a measurement in which they observed an abnormally large annihilation rate for large molecules. These phenomena were first interpreted as a temporal attachment of an incoming positron to neutral molecules. However, some theoretical attempts to search for the positron attachment to small molecules were not successful. Later, more firmer and more direct evidence was observed by Surko and colleagues [103,104,139]. In their experiment, they claimed to discover that positrons can form a long-lived resonance state within large molecules like alkanes at the incident energy of a few tenth of eV, by examining time-of-flight (TOF) spectra of positive ions produced when a positron annihilates.

In the positron-TCSs obtained by the Sueoka group, as has been discussed above, a rather distinct peak or a small hump, depending upon the molecule, is found around the 1–2 eV particularly for large molecules such as alcohol, acid and freon gases. We believe that these peaks could be strong candidates for providing evidence of positron attachment, since these large molecules can readily hold the incoming positron within a molecule by absorbing the extra kinetic energy. Eventually, of course, the trapped positron will either escape through the tunneling effect, leaving a neutral molecule behind, or annihilate by emitting the gamma ray, leaving a positive molecular ion behind. If this mechanism is indeed possible, then it may be useful because fragile molecular ions can rather easily be obtained using it. Molecular ions are not obtainable by conventional methods like electron impact ionization. In the production of molecular ions through electron impact ionization, because of the violent impulsive impact, the resulting ions are often in an excited state both in electronic and in nuclear states, leading to a short lifetime of molecular ion. In contrast, the molecular ion produced through the positron attachment may have a long life and be likely to exist in both the electronic and nuclear ground states. In addition, this method can be used for an analysis of unknown molecular species in conjunction with mass spectrometry and can give an insight into molecular-fragmentation dynamics, as well. However, a more direct measurement of the positron attachment is certainly necessary for further understanding of the mechanism along with the help of theoretical interpretation.

Recently, very intriguing phenomena have been observed by Sueoka and Kimura [64] on the relationship between Ps formation and TCS, or the

contribution of Ps formation to the total cross section. The experimental results are tabulated in Table III. In the table, the ratio of Ps formation cross section to the TCS, evaluated at 2 eV above the respective Ps-formation thresholds, is given for various molecules. As observed, these ratios have very conspicuous and perhaps important features, which are summarized here: (1) the ratio is found to be rather large for systems which have a C–H bond; (2) the ratio is small for those molecules which contain a C–F bond; (3) in hydrocarbons, the ratio is small for those which have double and triple bonds, compared to those with single bonds; (4) the ratio becomes larger for simpler molecules (smaller-size molecules); and (5) the ratio is generally found to be small for polar molecules. Qualitatively, it is suggested that when molecular electron clouds are tightly bound within a molecule and do not "leak out" far from the molecule, or in other words, when electrons are more closely localized near nuclei, then a positronium is less likely to be formed [see specifically the cases (1), and (3), above]. As stated above, for these molecules, which have many electrons (larger molecules) and are spatially spread out, there are more chances to form resonances (positronium-in-molecule) rather than Ps formation, substantially reducing the ratio for these larger molecules. There seems to exist a relationship between these ratios and molecular properties such as the dipole moment. Nevertheless, further theoretical investigations are needed to make more definite arguments based on these findings [7].

F. Positron–Surface Interactions and Positron Slowing-Down in Condensed Phase

Positron and electron interactions with solid surfaces and their penetration into condensed phases are somewhat remote from the main scope of this review. However, they closely relate to electron– and positron–polyatomic molecule scattering in a gas phase, and hence some remarks are warranted, which it is hoped will help to provide a more comprehensive view of the subject.

In order for an electron to be released from solid surface, it requires an extra external energy equivalent to its work function, while for positron, its work function is negative, and hence a positron is pushed out near the surface without costing any extra energy. This difference is significant and essential for discriminating the two schemes of dynamics, and is also important for various applications. If a positron is introduced into a bulk solid and is trapped inside, it is likely to move around within the solid, and gather and settle down at a defect or in a top-layer of the surface. Therefore, by using the positron measurement technique, information on the lattice defect and surface properties can be attained. Further, if a positron is trapped inside one of atomic holes in the solid, it tends to annihilate through

interaction with an outer-shell electron whose kinetic energy is small. The γ-ray thus emitted from the annihilation lies in a narrow peak at 511keV. Using a high-resolution angular correlation spectroscopy, it is possible to determine the rate of the hole creation in solid surface or bulk properties. There are a few other advantages of using a positron beam over the electron counterpart for investigating solid properties. Knowledge of positron–molecule scattering dynamics provides firm basis for understanding positron–solid scattering dynamics [140–142].

If an energetic positron is introduced into liquid or solid phases, it slows down by giving off its kinetic energy through frequent elastic as well as inelastic collisions with constituent atoms and molecules [143]. At the end of its track or path, its kinetic energy becomes equivalent to the thermal one, and the electron or positron is trapped and annihilates within an order of nano-seconds for the case of positron. However, before it annihilates, it ionizes, and excites constituent atoms and molecules or forms positronium, inducing various chemical processes in liquid within a narrow spatial region. This region is sometimes called a spur in radiation chemistry and physics, and the study of various reactions taking place inside the spur is important for understanding Ps formation as well as the basic radiation chemistry. For the slowing-down process, it is known that electrons and positrons show a different behavior due to the sign of the charge. For example, for electron slowing-down, an incoming electron repels target electrons, reducing the rate of the energy-loss process, while for positron slowing-down, the incoming positron attracts target electrons, and these target electrons "swarm" toward the positron to increase collisions and hence the energy loss. Therefore, the so-called stopping cross section or stopping power is different for the two projectiles, and in addition, the size of the track and the thermalization distance and time are apparently different [143]. The difference between the positron spur and that of the electron is considered to be significant for providing further understanding of radiation chemistry and biology.

Finally, the scavenger effect of positron penetration in liquid is also interesting and important. Depending upon the strength of electron scavenging, addition of molecules like CCl_4 and C_2H_5Br into liquid is known to reduce Ps formation, while if C_6F_6 or anthracene are added, they increase Ps formation. These observations can be interpreted to indicate that some scavengers hold the electron long enough to avoid annihilation. This phenomenon may share the same origin of dynamics with that described for the relationship between Ps formation and TCSs [64]. A comparative study of collisions of electron and positron with polyatomic molecules undoubtedly thus serves as a basis for providing much insight into positron chemistry.

V. CONCLUDING REMARKS

Positron beams are becoming increasingly important in various basic sciences as well as in applied fields. To name but a few immediate applications, they are expected to provide: (1) detailed information of lattice defects of thin films or bulk solids such as semiconductors, provided by the measurement of the Doppler width of the annihilation gamma rays; (2) means for determining structures of complex biological molecules by the observation of positron annihilation or positronium formation, or by more precise measurements performed on chemical reactions; (3) selective destruction of DNA molecules in a biological system to investigate a sudden mutation in a living cell; and (4) means to test the precision of quantum electro dynamics (QED). Furthermore, it has recently been suggested that a comparison of the γ-ray emission through positron annihilation with that originating from the galactic center will provide necessary clues to the birth of the universe or the Big-bang theory. Of course, the positron emission tomography (PET) is now a valuable addition to medical diagnosis, as well as to basic biological and medical research in such areas as human-body metabolism in brains. For all these applications, a comparative understanding of interactions and dynamics between electron and positron impacts on polyatomic molecules constitutes a basic foundation without which any further progress would not be possible.

In this comparative study between electron and positron impacts, it is apparent that a few very important aspects of new physics and chemistry have clearly emerged, but at the same time, a number of new questions have also arisen that need to be answered. These points of inquiry certainly help to further clarify the present understanding of electron and positron interaction mechanisms and scattering dynamics. At the same time, they also indicate the future direction of research. Therefore, to provide a synopsis some of the important findings and problems are summarized below, even though some are perhaps too closely interrelated to be neatly itemized.

(1) For polar molecules with a sizable dipole moment, TCSs for both electron and positron impacts are comparable or very close in magnitude, and show a similar trend as a function of the scattering energy. This phenomenon can be understood as confirming the effect of long-range dipole interaction, which in turn renders irrelevant the question as to whether or not the projectile can actually penetrate inside a molecule.

(2) For diatomic molecules, a rather sharp increase in the total cross section due to positronium formation, identifiable as the threshold structure, is clearly visible. However, as the size of a molecule increases, this structure due to positronium formation weakens, suggesting that the positronium

formation is less effective. This probably relates to the fact that the overall positron interaction potential (the sum of the static and correlation–polarization potentials) has a shallow well [see Fig. 11(a) and (b)], and that the number of wells increases as the molecular size (the number of atoms) increases. Then the incoming positron is more likely to be temporarily captured within one of the wells to form a shape resonance (positron-in-molecule).

(3) For all molecules, the electron TCS is uniformly larger than that for positrons, in the intermediate scattering energy region ranging roughly from 3–4 eV to a few hundred eV, where both TCSs begin to merge. This difference is generally attributable to a weaker interaction for a positron than that for an electron. However, in the energy region below the electronic excitation threshold but well above the vibrational excitation threshold, or the energy region where the Ramsaur–Townsend minimum occurs, ($2 \sim 3$ eV) the positron-TCS for some molecules becomes larger than that for electron impact. Considering the energy region where the reverse of the TCS occurs, the origin of this phenomenon should be due to rovibrational excitation or positron attachment. This phenomenon has been seen both for polar molecules and for nonpolar molecules, as described in Section IV.A, but no systematics is yet clearly understood with respect to the molecular type. This reversal may have a significant effect in the area of applications. From the results of our study, it is clear that vibrational excitation for positron impact is normally smaller than that for electron impact, but for rotational excitation, positron impact sometimes gives a larger cross section than electron impact, as may be obvious from the Born argument in Eq. (3.31). Therefore, the larger rotational excitation cross section for positron impact may be responsible for this phenomenon in certain cases.

(4) In relation to (2) above, a few small structures can be seen in positron TCSs, particularly below 30–50 eV. The number of structures seems to increase as the number of constituent atoms increases, or the molecular size increases. These structures may well be due to the shape resonance (a positron-in-molecule), or perhaps to a strong binding with the target electron charge cloud through the Coulomb attraction.

(5) The Ramsaur–Townsend (RT) effect has been observed in positron scattering from He and Ne, for which no RT effect is seen for electron impact. A similar RT effect should be seen for the molecules, for which the effect would not be possible by electron impact. Unfortunately, due to the experimental limitation, we have observed no clear evidence of that RT effect yet. This effect would be significant also from the point of view of applications.

(6) If a target molecule is in the singlet ground electronic state, no triplet state is formed through a positron impact because the electron exchange is completely absent in this collision. Since no positron–electron correlation is known at this time, we are unable to assess the magnitude of a spin–flip process for the triplet formation within the target through the correlation.

(7) Positron- and electron-TCSs begin to merge at around 100 eV for some molecules, while the merging energy appears to shift toward higher energies for some larger molecules. Even for a large-molecular group, the merging energy is not always unique, however. Hence, unfortunately we are unable to derive any systematics in regard to this phenomenon. The higher merging energy holds particularly true, however, when a heavier atom replaces a lighter one in the molecule; a good example is C_2H_6 vs. C_2F_6. This clearly suggests that the lowest-order Born approximation ceases to be appropriate, and certainly higher-order terms should be considered for the sake of a better description.

(8) Some of vibrational excitation cross sections are much smaller for positron scattering than for electron scattering. This smaller size depends on the sensitive balance between the coupling range and the penetration depth of the incoming electron or positron. As seen, CO_2 is an example of this strong mode-dependence for vibrational excitation, and, it has recently been extensively studied.

(9) The magnitude of rotational excitation cross section for electron and positron scattering depends on nature of the target, and varies from system to system. This aspect is markedly different from the vibrational excitation case and perhaps contributes to the reverse of the magnitudes of the TCSs between electron and positron impacts in the region below 2–3 eV. An additional contribution would be the attachment resonance.

(10) As seen in Table III, there seems to exist a systematic relationship between the cross section ratio of the Ps formation to TCS and molecular properties. Further systematic, comprehensive investigation would be highly desirable in order to elucidate this relationship.

(11) At an intermediate energy and above, experimental observations apparently suggest that ionization and electronic excitation cross sections for positron impact for some atomic and molecular targets are a few % to 15% larger than those for electron impact, though the total cross section for electron impact in the same energy domain is generally known to be appreciably larger than that for positron. If the existence of the larger cross sections for electronic excitation for positron impact is indeed proved to be true, then what is the dynamical mechanism which causes the difference? Also, what is the major contributor to causing the larger total cross section for electron impact? From our study, we now know that some vibrational

excitation cross section for electron impact is larger than that shown for positron impact. But can these vibrational excitations account for the greater part of the difference, combined with larger elastic cross section, as has been suggested theoretically by Dewangen and Walters [144] for atomic targets?

Attempting to answer the questions outlined above continues to pose major challenges to experimentalists and theorists alike, and the findings that will naturally follow from meeting these challenges surely have a strong potential to create a new research area of physics for atoms and molecules, for condensed matter as well as for exotic particles. Now, at various laboratories throughout the world, high-intensity and monochromatic positron beam lines for basic and applied sciences are either in the planning stages to be built, or are already under construction. With these new beam lines in hand, the hope of obtaining much finer information on electron and positron scattering dynamics will be a reality and hence help to resolve, perhaps in near future, the long-standing questions of the basic difference between electron–molecule and positron–molecule interactions and its relationship to the overall dynamical mechanism.

Acknowledgments

This project was supported in part by the grant from the Ministry of Education, Japan. The authors thank various colleagues who provided numerical data, figures, and suggestions for making this article more readable, and among those we would like to single out a few by name Tamio Nishimura, Michiya Takekawa, Steve Buckman, Cliff Surko, Alex Dalgarno, Bill Raith, and Walter Kauppila. We gratefully appreciate their help and support during the course of the writing. Mineo Kimura acknowledges the support of the Deutsche Akademische Austauschdienst (DAAD) through Universität Wuppertal during the time when much of this article was written.

References

1. K. Takayanagi and M. Inokuti, *J. Phys. Soc. Jpn.* **23**, 1412 (1967).
2. J. G. Lodge, J. W. Darewych, and R. P. McEachran, *Can. J. Phys.* **49**, 13 (1971).
3. S. Hara, *J. Phys.* B**7**, 1748 (1974).
4. P. G. Coleman, T. C. Griffith, and G. R. Heyland, *Appl. Phys.* **4**, 89 (1974).
5. J. W. Darewych, P. Baille, and S. Hara, *J. Phys.* B**7**, 2047 (1974).
6. E. A. G. Armour, *Phys. Rep.* **169**, 1 (1988).
7. G. Laricchia and C. Wilkin, *Phys. Rev. Lett.* **79**, 2241 (1997).
8. A. Jain, *J. Phys.* B**23**, 863 (1990).
9. A. Schwab, P. Honer, W. Raith and G. Sinapius, in *Atomic Physics with Positrons* (J. W. Humberston and E. A. G. Armour eds.), pp. 429, Plenum, New York, 1989.

10. M. Charlton and G. Laricchia, *J. Phys.* B**23**, 1045 (1990).
11. L. M. Diana, P. G. Coleman, D. L. Brooks, P. K. Pendleton and D. M. Norman, *Phys. Rev.* A**34**, 2731 (1986).
12. L. Dou, W. E. Kauppila, C. K. Kwan and T. S. Stein, *Phys. Rev. Lett.* **68**, 2913 (1992).
13. O. Sueoka, S. Mori and A. Hamada, *J. Phys.* B**27**, 1453 (1994).
14. W. E. Kauppila and T. S. Stein, *Adv. At. Mol. Opt. Phys.* **26**, 1, (1989).
15. D. A. Przybyla, W. Addo-Asah, W. E. Kauppila, C. K. Kwan, and T. S. Stein, *The Proceedings for Positron Workshop*, 1 (1997), Nottingham, UK.
16. M. Kimura, M. Takekawa, Y. Itikawa, H. Takaki and O. Sueoka, *Phys. Rev. Lett.* **80**, 3936 (1998).
17. J. Tennyson and L. Morgan, *J. Phys.* B**20**, L641 (1987).
18. G. Danby and J. Tennyson, *J. Phys.* B**24**, 3517 (1991).
19. J. S. E. Germano and M. A. P. Lima, *Phys. Rev.* A**47**, 3976 (1993).
20. J. L. S. Lino, J. S. E. Germano and M. A. P. Lima, *J. Phys.* B**27**, 1881 (1994).
21. F. A. Gianturco, P. Paioletti and J. A. Rodriguez-Ruiz, *Z. Phys.* D**36**, 51 (1996).
22. D. M. Schrader, F. M. Jacobsen, N.-P. Frandsen and U. Mikkenlsen, *Phys. Rev. Lett.* **69**, 57 (1992).
23. G. G. Ryzhikh and J. Mitroy, *Phys. Rev. Lett.* **79**, 4124 (1997).
24. M. A. Morrison, in *Positron (Electron)-Gas Scattering* (W. E. Kauppila, T. S. Stein and J. M. Wadehra eds.), World Scientific, Singapore, 1986.
25. E. W. McDaniel, *Atomic Collissions: Electron and Photon Projectiles*, John Wiley & Sons, Inc., New York, 1989.
26. H. Tawara, Y. Itikawa, H. Nishimura and M. Yoshino, *J. Phys. Chem. Ref. Data*, **19**, 617 (1990).
27. K. F. Canter, P. G. Coleman, T. C. Griffith and G. R. Heyland, *J. Phys.* B**5**, L167 (1972).
28. T. S. Stein and W. E. Kauppila, *Adv. At. Mol. Phys.* **18**, 53 (1982).
29. W. E. Kauppila and T. S. Stein, *Can. J. Phys.* **60**, 471 (1982).
30. J. M. Dale, L. D. Hulett and S. Pendyala, *Surf. and Interface Anal.* **2**, 199 (1980).
31. T. C. Griffith, *Adv. At. Mol. Phys.* **15**, 135 (1979).
32. P. G. Coleman, J. D. McNutt, L. M. Diana and J. T. Hutton, *Phys. Rev.* A**22**, 2290 (1980).
33. G. Sinapius, W. Raith and W. G. Wilson, *J. Phys.* B**13**, 4079 (1980).
34. O. Sueoka and S. Mori, *J. Phys. Soc. Jpn.* **53**, 2491 (1984).
35. O. Sueoka and S. Mori, *J. Phys.* B**19**, 4035 (1986).
36. S. Mori and O. Sueoka, *J. Phys.* B**27**, 4349 (1994).
37. P. G. Coleman, T. C. Grifith and G. R. Heyland, *Appl. Phys.* **5**, 223 (1974).
38. K. R. Hoffman, M. S. Dababneh, Y.-F. Hsieh, W. E. Kauppila, V. Pol, J. H. Smart and T. S. Stein, *Phys. Rev.* A**25**, 1393 (1982).
39. A. Hamada and O. Sueoka, *J. Phys.* B**27**, 5055 (1994).
40. A. Hamada, Ph.D. thesis, Yamaguchi University, Ube, Japan, 1994.
41. Y. Okamoto, K. Onda and Y. Itikawa, *J. Phys.* B**26**, 745 (1993).
42. T. C. Griffith, G. R. Heyland, K. S. Lines and T. R. Twomey, *J. Phys.* B**12**, L747 (1979).
43. P. G. Coleman and J. T. Hutton, *Phys. Rev. Lett.* **45**, 2017 (1980).
44. O. Sueoka, *J. Phys. Soc. Jpn.* **51**, 2381 (1982).
45. V. Katayama, O. Sueoka and S. Mori, *J. Phys.* B**20**, 1645 (1987).

46. O. Sueoka and S. Mori, *At. Col. Res: Jpn.* **12**, 18 (1986).
47. M. Tronc, A. Hitchcock and F. Edard, *J. Phys.* B**22**, L207 (1989).
48. D. Fromme, G. Kruse, W. Raith and G. Sinapius, *Phys. Rev. Lett.* **57**, 3031 (1986).
49. J. Moxom, G. Laricchia and M. Charlton, *J. Phys.* B**28**, 1331 (1995).
50. P. Ashley, J. Moxom and G. Laricchia, *Phys. Rev. Lett.* **77**, 1250 (1996).
51. H. Klar, *J. Phys.* B**14**, 4165 (1981).
52. W. Ihra, J. H. Macek, F. Mota-Furtado and P. F. O'Mahony, *Phys. Rev. Lett.* **78**, 4027 (1997).
53. M. Charlton, T. C. Griffith, G. R. Heyland, K. S. Lines and G. L. Wright, *J. Phys.* B**13**, L757 (1980).
54. L. S. Fornari, L. M. Diana and P. G. Coleman, *Phys. Rev. Lett.* **51**, 2276 (1983).
55. L. M. Diana, P. G. Coleman, D. L. Brooks, P. K. Pendleton and D. M. Norman, *Phys. Rev.* A**34**, 2731 (1986).
56. D. Fromme, G. Kruse, W. Raith and G. Sinapius, *J. Phys.* B**21**, L261 (1988).
57. L. S. Fornari, L. M. Diana and P. G. Coleman, *Phys. Rev. Lett.* **51**, 2276 (1983).
58. R. W. Bussard, R. Ramaty and R. J. Drackman, *Astrophys. J.* **228**, 928 (1979).
59. C. K. Kwan, H. Li, W. E. Kauppila, S. Nazaran, N. Scahill, T. S. Stein and S. Zhou, The book of abstract, ICPEAC TH077 (1997).
60. S. Zhou, H. Li, W. E. Kauppila, C. K. Kwan and T. S. Stein, *Phys. Rev.* A**55**, 361 (1997).
61. M. Charlton, G. Clark, T. C. Griffith and G. R. Heyland, *J. Phys.* B**16**, L465 (1983).
62. R. I. Campeanu, D. Fromme, G. Kruse, R. P. McEachran, L. A. Parcell, W. Raith, G. Sinapius and A. D. Stauffer, *J. Phys.* B**20**, 3557 (1987).
63. W. E. Meyerhof and G. Laricchia, *J. Phys.* B**30**, 2221 (1997).
64. O. Sueoka and M. Kimura, *Phys. Rev. Lett.* **xx**, xxx (2000).
65. G. M. A. Hyder, M. S. Dababneh, Y.-F. Hsieh, W. E. Kauppila, C. K. Kwan, M. Mahdavi-Hezaveh and T. S. Stein, *Phys. Rev. Lett.* **57**, 2252 (1986).
66. D. A. Przybyla, W. E. Kauppila, C. K. Kwan, S. J. Smith and T. S. Stein, *Phys. Rev.* A**55**, 4244 (1997).
67. L. Boesten and H. Tanaka, *J. Phys.* B**24**, 821 (1991).
68. T. Sakae, S. Sumiyoshi, E. Murakami, Y. Matsumoto, K. Ishibashi and A Katase, *J. Phys.* B**22**, 1385 (1989).
69. A. Jain and F. A. Gianturco, *J. Phys.* B**24**, 2387 (1991).
70. P. G. Coleman, J. D. McNutt, J. T. Hutton, L. M. Diana and J. L. Fry, *Rev. Sci. Instrum.* **51**, 935 (1980).
71. W. E. Frieze, D. W. Gidley and K. G. Lynn, *Phys. Rev.* B**31**, 5628 (1985).
72. N. F. Lane, *Rev. Mod. Phys.* **52**, 29 (1980). G. Laricchia, M. Charlton, C. D. Beling and T. C. Griffith, *J. Phys.* B**20**, 1865 (1987).
73. C. Winstead and V. McKoy, *Adv. Chem. Phys.* **XCVI**, 103 (1996).
74. T. N. Rescigno, B. H. Lengsfield and C. W. McCurdy, in *Modern Electronic Structure Theory*, D. F. Yarkony, ed. p. 501, World Scientific, Singapore, 1995.
75. E. P. Wigner, *Phys. Rev.* **70**, 15 (1946).
76. P. G. Burke, A. Hibbert and W. D. Robb, *J. Phys.* B**4**, 153 (1971).
77. P. G. Burke and W. D. Robb, *Adv. At. Mol. Phys.* **11**, 143 (1975).
78. P. G. Burke, *Adv. At. Mol. Phys.* **15**, 471 (1979).

79. B. I. Schneider, in *Computational Methods for Electron-Molecule Collisions* (W. M. Huo and F. A. Gianturco eds.), Plenum Press, New York, 1995.
80a. P. G. Burke and K. A. Berrington, *R-Matrix Theory of Atomic and Molecular Processes* IOP Publishing, Bristol, U.K. 1993.
80b. W. E. Kauppila, C. K. Kwan, D. Przybyla, S. J. Smith and T. S. Stein, *Can. J. Phys.* **74**, 474 (1996).
81. D. Dill and J. L. Dehmer, *J. Chem. Phys.* **61**, 692 (1974).
82. M. Kimura and H. Sato, *Comment At. Mol. Phys.* **26**, 333 (1991).
83. J. L. Dehmer, J. Siegel and D. Dill, *J. Chem. Phys.* **69**, 5205 (1978).
84. J. L. Dehmer, in "*Electron-Molecule and Photon-Molecule Collisions*" (T. Rescigno, V. McKoy and B. Schneider eds.), Plenum Press, 1984.
85. H. Sato, M. Kimura and K. Fujima, *Chem. Phys. Lett.* **145**, 21 (1988).
86. E. Boronski and R. M. Nieminen, *Phys. Rev.* B**34**, 3820 (1986).
87. N. T. Padial and D. W. Norcross, *Phys. Rev.* A**29**, 1742 (1984).
88. K. Onda and D. G. Truhlar, *J. Chem. Phys.* **72**, 1415 (1980).
89. J. C. Slater, *Quantum Theory of Atomic Structure* (McGraw-Hill, NL, 1960).
90. S. Hara, *J. Phys. Soc. Jpn.* **22**, 710 (1967).
91. T. Nishimura, Proceedings on Workshop for Atomic and Molecular Processes in Low-Temperature Plasma, ISAS, P. 104 (1999).
92. A. Öre, Naturvidenskap Rikke No. 9, Univ. of Bergen, Årbok (1949).
93. J. S. Briggs and J. H. Macek, *Adv. At. Mol. Opt. Phys.* **28**, 1 (1991).
94. M. Kimura and N. F. Lane, *Adv. At. Mol. Opt. Phys.* **26**, 76 (1989).
95. O. H. Crawford and A. Dalgarno, *J. Phys.* B**4**, 494 (1971).
96. Y. Itikawa, *Int. Rev. Phys. Chem.* **16**, 155 (1997).
97. S. Altshuler, *Phys. Rev.* **107**, 114 (1957).
98. N. F. Mott and H. S. W. Massey, *The Theory of Atomic Collisions* Oxford University, Press, London, 1974.
99. M. A. Morrison, *Adv. At. Mol. Phys.* **24**, 51 (1987).
100. Y. Nakamura, *Aust. J. Phys.* **48**, 357 (1995).
101. H. Massey, *Physics Today*, 42 (Mar. 1976).
102. D. A. L. Paul and L. Saint-Pierre, *Phys. Rev. Lett.* **11**, 493 (1963).
103. C. M. Surko, A. Passner, M. Leventhal and F. J. Wysocki, *Phys. Rev. Lett.* **61**, 1831 (1988).
104. K. Iwata, R. G. Greaves, T. J. Murphy, M. D. Tinkle and C. M. Surko, *Phys. Rev.* A**51**, 473 (1995).
105. J. Xu, L. D. Hulett, Jr., T. A. Lewis, D. L. Donohue, S. A. McLuckey and O. H. Crawford *Phys. Rev.* A**49**, R3151 (1994).
106. K. Higgins and P. G. Burke, *J. Phys.* B**26**, 4269 (1993).
107. O. Sueoka, S. Mori and Y. Katayama, *J. Phys.* B**19**, L373 (1986).
108. O. Sueoka, S. Mori and Y. Katayama, *J. Phys.* B**20**, 3237 (1987).
109. A. Jain, *J. Phys.* B **19**, L105 (1986).
110. A. Jain and D. G. Thompson, *Phys. Rev.* A**30**, 1098 (1984).
111. M. G. Lynch, D. Dill, J. Siegel and J. L. Dehmer, *J. Chem. Phys.* **71**, 4249 (1979).
112. M. Takekawa and Y. Itikawa, *J. Phys.* B**31**, 3245 (1998).

113. M. Takekawa and Y. Itikawa, *J. Phys.* B**32**, 4209 (1999).
114. F. A. Gianturco, T. Mukherjee and P. Paioletti, *Phys. Rev.* A**56**, 3638 (1997).
115. M. Kimura, O. Sueoka, A. Hamada, M. Takekawa, Y. Itikawa, H. Tanaka and L. Boesten, *J. Chem. Phys.* **107**, 6616 (1997).
116. O. Sueoka, H. Takaki, A. Hamada, H. Sato and M. Kimura, *Chem. Phys. Lett.* **288**, 124 (1998).
117. H. Tanaka, Y. Tachibana, M. Kitajima, D. Sueoka, H. Takaki, A. Hamada and M. Kimura, *Phys. Rev.* A**59**, 2006 (1999).
118. H. Tanaka, T. Masai, M. Kimura, T. Nishimura and Y. Itikawa, *Phys. Rev.* A**56**, R3338 (1997).
119. A. Jain, *J. Phys.* B**19**, L379 (1986).
120. A. Jain, *Phys. Rev.* A**35**, 4826 (1987).
121. O. Sueoka and S. Mori, *J. Phys.* B**22**, 963 (1989).
122. K. Floeder, D. Fromme, W. Raith, A. Schwab and G. Sinapius, *J. Phys.* B**18**, 3347 (1985).
123. A. M. Frolov and V. H. Smith, Jr., *Phys. Rev.* A**55**, 2662 (1997).
124. O. Sueoka, *J. Phys. B***21**, L631 (1988).
125. D. A. Przybyla, W. Addo-Asah, W. E. Kauppila, C. K. Kwan and T. S. Stein, *Phys. Rev. A***60**, 359 (1999).
126. A. Kövér and G. Laricchia, *Phys. Rev. Lett.* **80**, 5309 (1998).
127. A. Jain, *J. Chem. Phys.* **86**, 1289 (1987).
128. J. Tennyson, *J. Phys.* B**19**, 4255 (1986).
129. T. Falke, W. Raith, M. Weber and U. Wesskamp, *J. Phys.* B**28**, L505 (1995).
130. A. Schmitt, U. Cerry, H. Möller, W. Raith and M. Weber, *Phys. Rev.* A**49**, R5 (1994).
131. T. Falke, T. Brandt, O. Kühl, W. Raith and M. Weber, *J. Phys.* B**30**, 3247 (1997).
132. H. Knudsen and J. Reading, *Phys. Rep.* **212**, 108 (1992).
133. H. Knudsen, et al. *J. Phys.* B**23**, 3955 (1990).
134. T. Mukherjee, S. Sur, and A. S. Ghosh, *J. Phys.* B**24**, 1449 (1991); *J. Phys.* B**24**, 3905 (1991).
135. M. A. Khakoo and J. Segura, *J. Phys.* B**27**, 2355 (1994).
136. S. J. Gilbert, R. G. Greaves and C. M. Surko, *Phys. Rev. Lett.* **82**, 5032 (1999).
137. A. Jain, *J. Phys.* B**19**, L807 (1986).
138. L. A. Morgan, *J. Phys.* B**19**, L439 (1986).
139. A. Passner, C. M. Surko, M. Leventhal and A. P. Mills, Jr., *Phys. Rev.* A**39**, 3706 (1989).
140. A. Rich, *Rev. Mod. Phys.* **53**, 127 (1981).
141. H. J. Ache, in *Positronium and Muonium Chemistry*, American Chemical Society Press, Washington, D. C., 1979.
142. K. G. Lynn, W. E. Frieze and P. J. Schultz, *Phys. Rev. Lett.* **52**, 1137 (1984).
143. J. C. Ashley, J. Elect. Spectro. Related Phenom. **50**, 323 (1990).
144. D. P. Dewangen and H. R. J. Walters, *J. Phys.* B**10**, 637 (1977).